shown. The absorbance values are expressed as mean ± SD relative to the absorbance values of untreated control ScMG20 cells from 3 independent experiments. Significant differences at $p<0.05$ (*) and 0.01 (**) between treated and untreated cells are indicated. (D) Structures of Brilliant Blue G. (E) Kaplan–Meier survival analysis of *tga20* mice inoculated with ScMG20 cells treated with or without BBG. *tga20* mice were inoculated intracerebrally with ScMG20 cells in 5 serial passages in the presence or absence of 30 μM BBG. Animals that received BBG-treated cells (BBG+, broken line) showed longer survival times compared to those that received untreated cells (BBG−, solid line). The inset picture shows that the kinetics of PrPres levels in ScMG20 cells serially passaged 5 times in the presence or absence of 30 μM BBG. The numbers above the lanes indicate the passage number.
doi:10.1371/journal.pone.0037896.g001

the 10 inoculated mice not succumbing to the disease within 400 days after inoculation. We also examined the efficacy of anti-prion activity of BBG using neuronal derivative N2a cells infected with the Chandler murine strain of scrapie (ScN2a). BBG also prevented PrPres accumulation in ScN2a cells, with an IC50 of 3.2 μM (data not shown).

BBG depletes cells of PrP and modifies its cellular localization

The level of endogenous PrPsen influences the rate of replication of prions [32] and a reduction in its level abrogates PrPres formation [33]. To examine whether the reduction of PrPres by BBG was mediated by the suppression of PrPsen, the PrPsen level in uninfected MG20 cells treated for 3 days with various concentrations of BBG was ascertained. Cell lysates not treated with proteinase K (PK) were subjected to western blotting, and the total PrPsen (full-length PrPsen plus C-terminal fragments) levels were determined after the removal of carbohydrates by PNGaseF (Fig. 2A). At a concentration of 60 μM, BBG significantly reduced the total PrP levels and mediated a reduction in the ratio of full-length PrPsen to total PrPsen, suggesting a preferential decrease in full-length PrPsen (Fig. 2B).

To determine whether BBG affected PrPsen synthesis, we examined the expression levels of PrPsen mRNA in MG20 cells treated with or without 30 μM BBG by Q-PCR. The PrPsen expression level was calculated as the ratio of the number of PrPsen copies to the number of GAPDH copies. The mean expression level of PrPsen in BBG-treated cells was 0.028±0.001 (mean ± SD of 3 independent experiments), which was slightly lower than that of 0.031±0.001 in untreated cells. This result suggests that the reduction of PrPsen might be, at least in part, associated with the downregulation of its expression.

PrPsen cycles between the cell surface and the endosomal compartments, and PrPres formation is postulated to occur in this pathway [34–38]. To determine whether BBG treatment can influence PrPsen localization, the cell-surface expression of PrPsen was investigated by fluorescence-activating cell sorting (FACS) analysis. Mabs 3H2, which reacts with linear amino acid epitope 38–53, was used to detect full-length PrPsen and Mabs T2, which reacts with the discontinuous epitope spanning amino acids 132–156, was used to assess the total PrPsen. BBG-treated cells showed a decrease in the level of full-length PrPsen levels on the cell surface as compared with untreated cells (Fig. 2C); this result was consistent with the western blotting results.

The effect of BBG on the cellular localization of PrPsen was also examined by confocal microscopy. To detect only full-length PrPsen, we used SAF32, which reacts with linear amino acid epitopes 59–89. In mock-treated non-permeabilized cells, full-length PrPsen was found to be localized at the cell surface. In the presence of BBG, a marked decrease of full-length PrPsen at the cell surface was detected (Fig. 2D). These results demonstrate that BBG interrupts the cell-surface expression of PrPsen.

Misfolded PrPsen is undetectable in BBG-treated cells

Previous studies have demonstrated that several anti-prion compounds cause misfolding of PrPsen, as evidenced by the relative detergent insolubility and formation of intracellular aggregates, resulting in the downregulation of surface PrPsen by altering its distribution inside the cell or inducing its rapid degradation (e.g., dextran sulfate, pentosan polysulfate, and epigallo catechin gallate) [26,39,40]. Thus, it is possible that the reduction in full-length PrPsen levels at the surface of BBG-treated cells is due to the misfolding of PrP.

To investigate this possibility, MG20 cells were treated with or without 30 μM BBG followed by a detergent solubility assay. Cells were lyzed in a detergent buffer, and the presence of PrPsen in the detergent-soluble and detergent-insoluble fractions was analyzed by western blotting. PrPsen was detected in both the detergent-soluble and, to some extent, the detergent-insoluble fractions (Fig. 3A). There was no significant difference in the level of detergent insoluble PrPsen in the presence or absence of BBG. Furthermore, the cellular localization of PrPsen in BBG-treated cells was visualized by indirect immunofluorescence of permeablized cells. Similarly, there was no observable difference in the intracellular localization of PrPsen in presence or absence of BBG (Fig. 3B).

BBG does not affect PrPres amplification in vitro.

To assess the possibility of the direct influence of BBG on PrPres formation, we utilized the PMCA technique [41]. PMCA was performed with chandler-infected mouse brain homogenate as the seed in the presence of BBG. For evaluating the amplification of PrPres after the PMCA reaction, the PK-resistant bands were semi-quantified by densitometric analysis. The presence of BBG in the PMCA reaction buffer did not significantly affect the amplification of PrPres except at an extremely high concentration (600 μM) (Fig. 4). These results suggest that BBG exert its effect on PrPres accumulation via complex cellular processes.

BBG reduces the cerebral accumulation of PrPres but does not prolong the survival time of murine GSS-infected mice

Lastly, we tested whether BBG could affect prion disease and prevent the disease progression during the later stages of infection. Hundred days after intracerebral inoculation with a high dose of FK-1 murine GSS strain (at 60% disease duration), mice were intraperitoneally treated with 100 mg/kg BBG 3 times per week for 3 weeks. In order to assess the effect of BBG on the pathological brain changes, some of the treated mice (n = 3) were euthanized and their brain homogenates were subjected to semi-quantitative western blotting at 121 days after infection (Fig. 5A, 5B). The remaining mice (n = 7) were continuously treated with 100 mg/kg BBG 2 times per week for a total of 7 weeks. In the brains of the mice treated with BBG for 3 weeks, the PrPres signal obtained using mAb T2 was reduced by 43% compared with that in the vehicle-treated control animals ($p<0.01$).

It has been shown that in murine prion disease, impaired synaptic protein, synaptic loss, and gliosis occur at an early stage [42–46]. Thus, the extent of synaptic loss and gliosis usually reflects the severity of the prion disease. Consistent with these reports, western blotting of the brain homogenates from mice infected with FK-1 strain demonstrated that synaptophysin levels

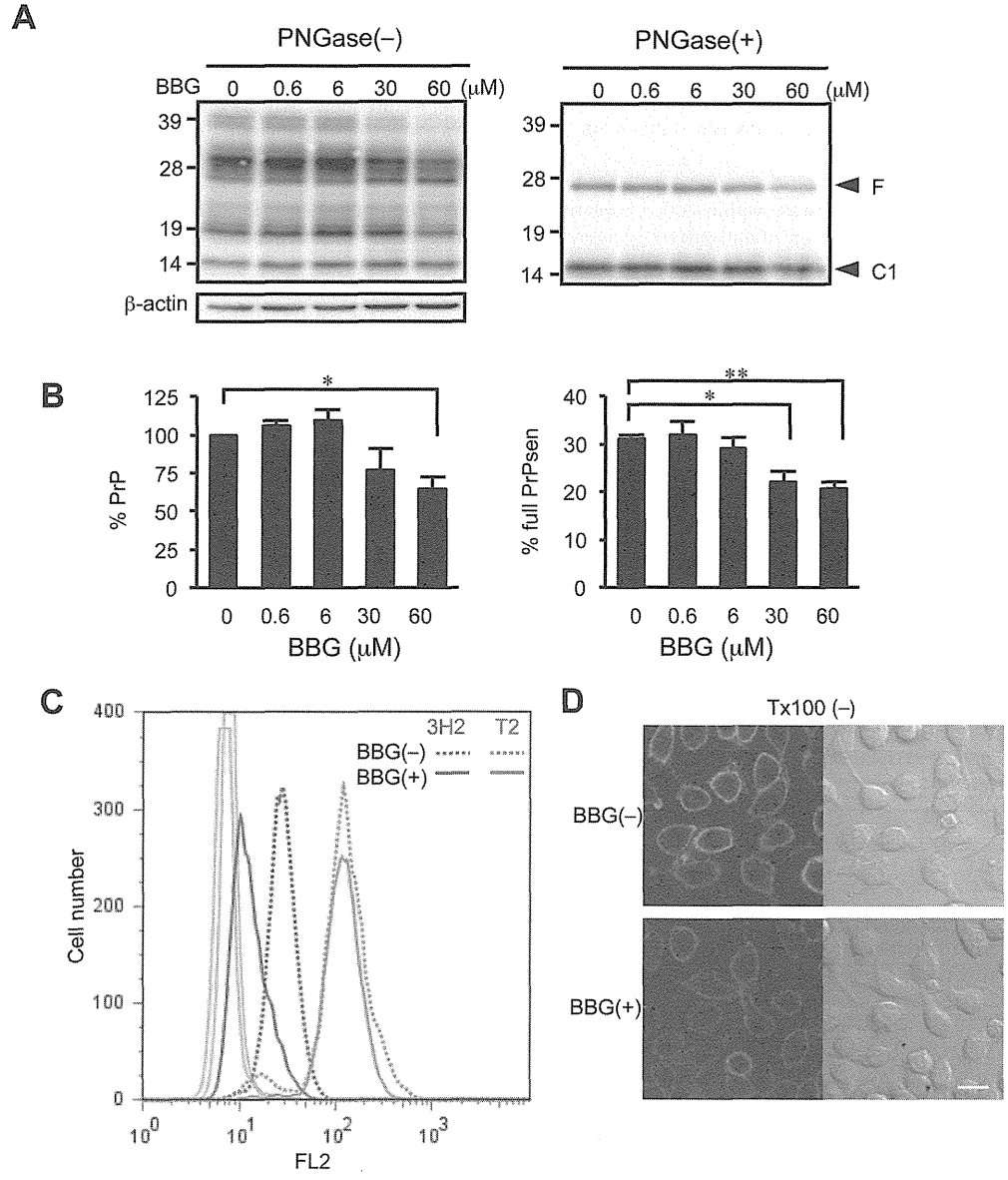

Figure 2. BBG depletes cells of PrPsen and mediates decrease in full-length PrPsen on cell surface. (A) Western blotting of the levels of PrPsen Uninfected MG20 cells were treated with or without 30 μM BBG for 3 days. PrPsen protein levels in MG20 cells were measured by western blotting. Molecular mass standards (kDa) are indicated on the left. The locations of full-length (F) and N-terminal truncated PrPsen (C1) are indicated. Membranes were probed with anti-β-actin to correct for any possible deviation on protein concentration. (B) The densitometric measurement of PrPsen signals detected in the blots after deglycosylation. The signals of PrPsen from BBG-treated cells are expressed as percentage of the signals from untreated cells (left panel). The signals of full-length PrPsen band intensities are expressed as a percentage of the signals from total PrPsen (full-length PrPsen plus C-terminal fragments) (right panel). Each bar indicates the mean values (±SD) of at least three independent experiments. Significant differences at $p<0.05$ (*) and $p<0.01$ (**) between BBG and untreated cells are indicated. (C) Fluorescence-activated cell sorting analysis of cell-surface expression levels of total PrPsen and full-length PrPsen of MG20 cells. The histograms depict the cell-surface expression in non-permeabilized cells incubated with 30 μM BBG for 3 days. FL2 represents the fluorescence intensity in BBG-treated cells (solid line) and in the untreated cells (dashed line), plotted against the number of cells (events). For each cell population, 10,000 events were measured. Mabs 3H2 was used for detection of full-length PrPsen (blue line), and Mabs T2 was used for detection of the total PrPsen (red line) on the cell surface. (D) Confocal fluorescence microscopic analysis of full-length PrPsen on the cell surface of MG20 cells. Cells were incubated with or without 30 μM BBG for 3 days. MG20 cells growing on cover glasses were fixed with 4% paraformaldehyde. Confocal fluorescent images (left panels) and Nomarski differential interference contrast images (right panels) were obtained. Scale bar, 20 μm.
doi:10.1371/journal.pone.0037896.g002

were decreased by approximately 30% and GFAP and Iba1 levels were elevated by approximately 310% and 230%, respectively, compared with those in mock-treated control mice. In accordance with a previous report [20], P2X7R levels were elevated by approximately 30% in diseased mice.

Surprisingly, in mice infected with FK-1 and treated with BBG, synaptic loss (synaptophysin marker) and astrogliosis (GFAP

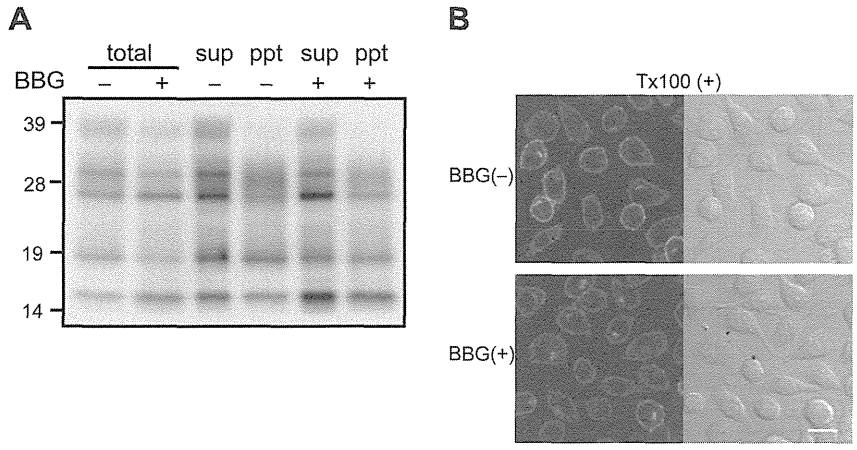

Figure 3. BBG does not induce formation of the detergent-insoluble PrPsen and the intracellular aggregated PrPsen. (A) Insoluble PrPsen detection in MG20 cells by detergent solubility assay. After incubation with or without 30 μM BBG for 3 days, cells were lyzed and postnuclear lysates were adjusted to 1% N-lauryl sarcosyl and ultracentrifuged for 1 h at 100,000× *g*. PrPsen present in the detergent-soluble (sup) and detergent-insoluble (ppt) fractions was analyzed by western blotting using monoclonal antibody T2. (B) Confocal fluorescence microscopic analysis of permeabilized MG20cells. Cells were incubated with or without 30 μM BBG for 3 days. MG20 cells growing on cover glasses were fixed with 4% paraformaldehyde and incubated with 0.1% Triton X-100. Confocal fluorescent images (left panels) and Nomarski differential interference contrast images (right panels) were obtained. Scale bar, 20 μm.
doi:10.1371/journal.pone.0037896.g003

marker) were enhanced by 20% and 30%, respectively, despite the apparent reduction in the levels of PrPres. Microgliosis (Iba1 marker) tended to decrease, however the reduction was not significant. P2X7R levels were decreased by approximately 20%. As a BBG-treatment control, we examined levels of PrP, GFAP, Iba1 and synaptophysin in the brains of mock-infected mice treated with vehicle or BBG (100 mg/kg, 3 times per week for 3 weeks). No statistically significant differences in these protein levels between vehicle and BBG treated animals were observed, suggesting no detectable detrimental effect of BBG in healthy animals at this dosage (data not shown).

In the infected mice treated with BBG for 7 weeks, no significant delay in disease progression was observed (Table 1). In addition, the level of PrPres did not differ significantly between the BBG- and vehicle-treated mice at the end of the study (data not shown). These results suggest that BBG administration slows down PrPres accumulation in the brains, but has no therapeutic efficacy in a mouse model of GSS during the later stages of infection.

Discussion

We showed here that BBG, a P2X7R antagonist, prevented PrPres accumulation in prion-infected MG20 microglial (IC50 14.6 μM) and N2a neural (IC50 3.2 μM) cell lines. *In vivo* administration of BBG, which was predicted to exert both anti-prion and P2X7R antagonistic activities, reduced PrPres accumulation in the brains of mice with prion disease, but it did not appear to alleviate the disease progression.

Among the three P2X7R antagonists examined, only BBG inhibited PrPres accumulation in a dose-dependent manner and reduced prion infectivity in cultured cells. These results suggest that its anti-prion activity was derived from its molecular frameworks, which are analogous to the well-known anti-prion compounds, such as Congo red, suramin, and curcumin, and not from its P2X7R antagonistic activity.

Several mechanisms can account for the effect of BBG on prion replication. We propose that BBG mediated the removal of PrPsen

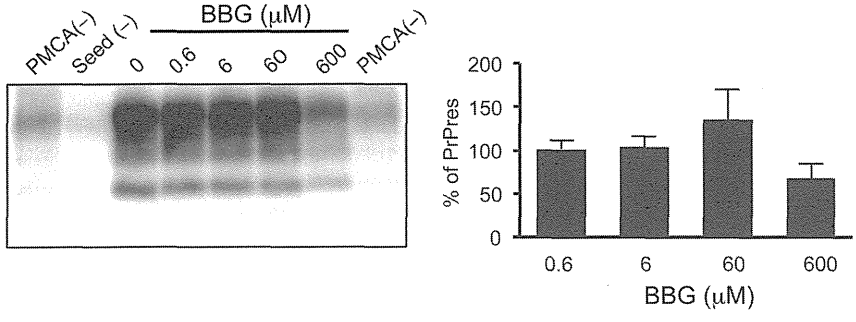

Figure 4. PrPres amplification in the presence of BBG by PMCA. (A) Western blotting of PrPres amplified by PMCA. The brain homogenates from mice with Chandler scrapie were added to normal mice brain homogenates to prepare final dilutions of 1:1000. PMCA was performed with BBG at indicated concentrations. After PK digestion, PrPres was detected by immunoblot with Mab T2. (0) represents samples without BBG, PMCA(−) represents samples without amplification and seed(−) represents samples for which PMCA was performed but without seed inoculumn. (B) Densitometric analysis of PK-resistant PrP signals in panel A. The signals of PrPres band intensities are expressed as a percentage of the PrPres signals from non-treated (0) cells. Each bar indicates the mean values (±SD) of at three independent experiments.
doi:10.1371/journal.pone.0037896.g004

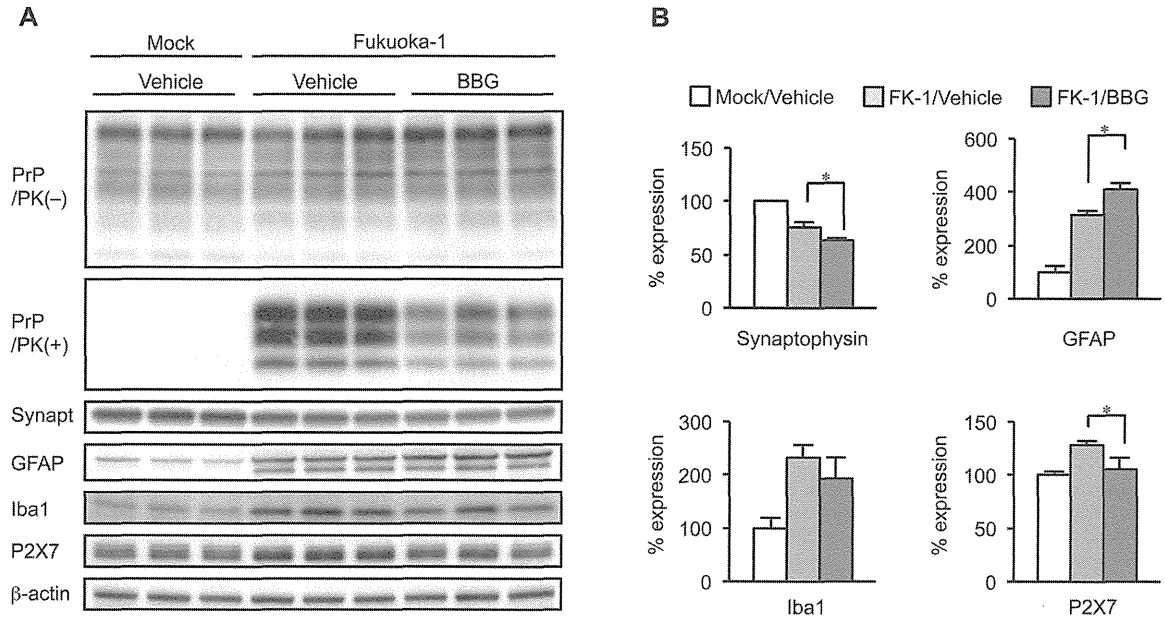

Figure 5. BBG prevents cerebral PrPres formation but not prevents disease progression. (A) Western blotting performed on the brain homogenates of Fukuoka-1 (FK-1) strain of murine GSS infected C57/BL6 mice treated with 100 mg/kg BBG for 3 times per week intraperitoneally for 3 weeks. The control mock and FK-1 infected animals were treated with the vehicle only. Membranes were probed with antibodies against indicated antigens. (B) Densitometric analysis of marker proteins in panel A. Each bar represents the average ratio from triplicate samples with mock-infected mice as standard. Significant differences at a $p<0.05$ (*) between the BBG- and vehicle-treated animals are indicated.
doi:10.1371/journal.pone.0037896.g005

from the plasma membrane and reduced the substrate for PrPres formation within the endocytic pathway. Numerous studies have shown that perturbation of PrPsen cellular trafficking results in inhibition of PrPres formation, indicating that PrPres formation happens either on the cell surface or along the endocytic pathway [34–38,47]. The manner in which BBG reduces the cell-surface PrPsen remains unclear. One possibility is that BBG might influence PrPsen synthesis. In uninfected MG20 cells, endogenous PrPsen levels were significantly reduced after incubation with BBG. In addition, there was a slight downregulation of PrPsen at the mRNA levels, which might explain the suppression of the cell-surface PrPsen.

Alternatively, BBG may directly interact with PrPsen on the cell surface or with other cellular components that influence PrPsen trafficking and accelerate the endocytosis of the cell-surface PrPsen. Several sulfated glycans decrease the amount of the cell-surface PrPsen by enhancing its rate of endocytosis through an unidentified mechanism associated with their binding to the N-terminal region of PrP, which is rich in basic amino acids and contains a consensus site for heparin and other sulfated glycans [40]. In addition, the conformational change or oligomerization of PrPsen at the cell surface induced by epigallocatechin gallate and copper lead to downregulation of cell-surface PrPsen [39,48]. Although a direct interaction between BBG and PrP remains to be confirmed, it is conceivable that the binding of BBG to the polybasic N-terminal of PrPsen could lead to its internalization since the interaction of BBG with proteins is known to be mediated by basic and aromatic amino acids [49]. On the other hand, a BBG-induced conformational change in PrPsen is unlikely since we did not detect structural alterations of PrPsen in the presence of BBG, which are characterized by the relative detergent insolubility and formation of intracellular aggregates.

The third possibility regarding the BBG-mediated reduction of cell-surface PrPsen is the enhanced degradation of PrPsen. The reduction of PrPsen levels can be mediated by induced lysosomal, proteasomal, and autophagic degradations of PrPsen under certain conditions [26,50,51]; there were not evaluated in this study. Whether BBG accelerates the degradation of PrPsen remains to be determined.

The anti-prion activity of BBG did not appear to relate to a destabilization of pre-existing PrPres aggregates. Incubation of the cell lysates with BBG before PK treatment did not reduce PrPres band intensity (data not shown). In addition, BBG did not significantly modify PrPres in the brain homogenates in a PMCA reaction. This observation excludes the possibility that BBG modifies the western blotting detection of PrPres due to an artifact.

Table 1. Effect of intraperitoneally administered BBG on animals cerebrally inoculated with Fukuoka-1 GSS strain.

Treatment	Mice (diseased/inoculated)	Mean incubation time (days ± SD)
Vehicle	7/7	161.9±5.5
BBG (100 mg/kg) starting at 100 dpi	7/7	163.3±5.0

dpi: days post inoculation.
doi:10.1371/journal.pone.0037896.t001

We hypothesized that BBG would display therapeutic efficacy against prion diseases *in vivo* based on its anti-prion activity and the neuroprotective effects of pharmacological antagonism of P2X7R reported in several animal models of neurodegenerative diseases. Unexpectedly, we demonstrated that BBG did not alleviate the progression of prion diseases. Two possibilities may explain the lack of neuroprotection following BBG administration, which was intended to pharmacologically antagonize P2X7R. It is most likely that activation of P2X7R plays an important role in neuroprotective effects under pathological conditions. Activation of P2X7R increases the production of endocannabinoids in microglial cells and astrocytes [13,14]. Sustained production of endocannabinoids reduces the release of glutamate and cytotoxic agents from neuron and microglia, respectively, and increases the release of growth factors, leading to neuroprotection [52–54]. Indeed, activation of cannabinoid receptors by cannabinoid derivatives mediates neuroprotection in animal models of prion disease [55]. Thus, it is conceivable that BBG might inhibit the neuroprotection pathways involving P2X7R by antagonizing this receptor.

A second possible explanation for the lack of a protective effect of BBG is that the effects of BBG may be attenuated by suppressed microglial inflammatory responses in prion diseases. It is widely accepted that over-activated microglia release potentially toxic products, including reactive oxygen species, excitotoxin, and proinflammatory cytokines such as interleukin (IL)-1β, IL-6, and tumor necrosis factor-α, and the P2X7R system is essential for the induction of microglial activation [9]. In the case of animal models of prion disease, despite marked astrocytosis and microglial activation, typical proinflammatory cytokine expression is absent or low at the protein level [56–58] compared with those induced by lipopolysaccharide. It has been proposed that such a suppressed inflammatory response is mediated by the downregulation of microglial responses by an antiinflammatory cytokine, such as transforming growth factor-β1 [59]. In addition, prion induced-glial cytokine responses are mainly mediated by astrocytes [56,57]. Taken together, we hypothesize that under such atypical inflammatory conditions characterized by restrained microglial response, BBG cannot exert neuroprotective effects because these effects have been attributed, at least in part, to its antiinflammatory activity of blocking microglial P2X7R [21]. This hypothesis is supported by previous results using an animal model of Parkinson's disease, where an atypical inflammatory response was observed [60] and pharmacological blockade of P2X7R by BBG and genetic deletion of this receptor had no protective effect on dopaminergic neurons [61]. Whether atypical inflammatory responses occurred in our mouse model of GSS remains to be determined. In addition, more research will be required to assess the correlation between the neuroprotective efficacy and antiinflammatory ability of BBG.

The change of brain pathology following BBG administration did not appear to relate to its potential toxicity of BBG. BBG is a derivative of a commonly used blue food dye (FD&C blue No. 1) and had been shown to be safe in healthy animals [62,63]. Furthermore, we preliminary compared levels of PrP, GFAP, Iba1 and synaptophysin between brains of mock-infected mice treated with vehiclle or BBG (100 mg/kg, 3 times per week for 3 weeks). No statistically significant differences in these protein levels between vehicle and BBG treated animals were observed (data not shown). These previous and our observations exclude the possibility that the potential toxicity of BBG influenced brain pathology in prion-diseased animals.

In summary, BBG prevented PrPres accumulation in both a cell culture and a mouse model of prion disease. Although BBG possessed anti-prion and highly selective P2X7R antagonistic activities, it did not appear to ameliorate the disease progression. This suggests that the observed P2X7R upregulation in the brains of diseased mice may play a neuroprotective role in prion disease. These results provide insight into the pathophysiology of prion diseases and have important implications for the treatment of these disorders. Despite the lack of a neuroprotective effect, BBG has many therapeutic advantages, including anti-prion activity, low toxicity, and permeability across blood–brain barrier. Therefore, continued study of BBG as a potential anti-prion compound is warranted, taking into consideration its antagonistic effect of P2X7R. Combining BBG and cannabinoids may prove effective in the treatment of prion-infected animals.

Acknowledgments

We are grateful to Yuko Miyama and Mariko Issiki for their technical assistance. We also thank the animal caretakers.

Author Contributions

Conceived and designed the experiments: YI TT HK. Performed the experiments: YI TT YM HO MI YS. Analyzed the data: YI TT MH SM TY HK. Wrote the paper: YI TT HK.

References

1. Prusiner SB (1991) Molecular biology of prion diseases. Science 252: 1515–1522.
2. Ferrari D, Villalba M, Chiozzi P, Falzoni S, Ricciardi-Castagnoli P, et al. (1996) Mouse microglial cells express a plasma membrane pore gated by extracellular ATP. J Immunol 156: 1531–1539.
3. Ballerini P, Rathbone MP, Di Iorio P, Renzetti A, Giuliani P, et al. (1996) Rat astroglial P2Z (P2X7) receptors regulate intracellular calcium and purine release. Neuroreport 7: 2533–2537.
4. Matute C, Torre I, Pérez-Cerdá F, Pérez-Samartín A, Alberdi E, et al. (2007) P2X(7) receptor blockade prevents ATP excitotoxicity in oligodendrocytes and ameliorates experimental autoimmune encephalomyelitis. J Neurosci 27: 9525–9533.
5. Deuchars SA, Atkinson L, Brooke RE, Musa H, Milligan CJ, et al. (2001) Neuronal P2X7 receptors are targeted to presynaptic terminals in the central and peripheral nervous systems. J Neurosci 21: 7143–7152.
6. Sperlágh B, Köfalvi A, Deuchars J, Atkinson L, Milligan CJ, et al. (2002) Involvement of P2X7 receptors in the regulation of neurotransmitter release in the rat hippocampus. J Neurochem 81: 1196–1211.
7. Marcoli M, Cervetto C, Paluzzi P, Guarnieri S, Alloisio S, et al. (2008) P2X7 pre-synaptic receptors in adult rat cerebrocortical nerve terminals: a role in ATP-induced glutamate release. J Neurochem 105: 2330–2342.
8. Papp L, Vizi ES, Sperlágh B (2004) Lack of ATP-evoked GABA and glutamate release in the hippocampus of P2X7 receptor−/− mice. Neuroreport 15: 2387–2391.
9. Monif M, Burnstock G, Williams DA (2010) Microglia: proliferation and activation driven by the P2X7 receptor. Int J Biochem Cell Biol 42: 1753–1756.
10. Ferrari D, Chiozzi P, Falzoni S, Hanau S, Di Virgilio F (1997) Purinergic modulation of interleukin-1 beta release from microglial cells stimulated with bacterial endotoxin. J Exp Med 185: 579–582.
11. Takenouchi T, Sugama S, Iwamaru Y, Hashimoto M, Kitani H (2009) Modulation of the ATP-Induced release and processing of IL-1beta in microglial cells. Crit Rev Immunol 29: 335–345.
12. Skaper SD, Facci L, Culbert AA, Evans NA, Chessell I, et al. (2006) P2X(7) receptors on microglial cells mediate injury to cortical neurons in vitro. Glia 54: 234–242.
13. Walter L, Dinh T, Stella N (2004) ATP induces a rapid and pronounced increase in 2-arachidonoylglycerol production by astrocytes, a response limited by monoacylglycerol lipase. J Neurosci 24: 8068–8074.
14. Witting A, Walter L, Wacker J, Möller T, Stella N (2004) P2X7 receptors control 2-arachidonoylglycerol production by microglial cells. Proc Natl Acad Sci U S A 101: 3214–3219.
15. Ortega F, Pérez-Sen R, Delicado EG, Teresa Miras-Portugal M (2011) ERK1/2 activation is involved in the neuroprotective action of P2Y(13) and P2X7 receptors against glutamate excitotoxicity in cerebellar granule neurons. Neuropharmacology.
16. Yiangou Y, Facer P, Durrenberger P, Chessell IP, Naylor A, et al. (2006) COX-2, CB2 and P2X7-immunoreactivities are increased in activated microglial cells/

macrophages of multiple sclerosis and amyotrophic lateral sclerosis spinal cord. BMC Neurol 6: 12.
17. Parvathenani LK, Tertyshnikova S, Greco CR, Roberts SB, Robertson B, et al. (2003) P2X7 mediates superoxide production in primary microglia and is up-regulated in a transgenic mouse model of Alzheimer's disease. J Biol Chem 278: 13309–13317.
18. McLarnon JG, Ryu JK, Walker DG, Choi HB (2006) Upregulated expression of purinergic P2X(7) receptor in Alzheimer disease and amyloid-beta peptide-treated microglia and in peptide-injected rat hippocampus. J Neuropathol Exp Neurol 65: 1090–1097.
19. Díaz-Hernández M, Díez-Zaera M, Sánchez-Nogueiro J, Gómez-Villafuertes R, Canals JM, et al. (2009) Altered P2X7-receptor level and function in mouse models of Huntington's disease and therapeutic efficacy of antagonist administration. FASEB J 23: 1893–1906.
20. Takenouchi T, Iwamaru Y, Imamura M, Kato N, Sugama S, et al. (2007) Prion infection correlates with hypersensitivity of P2X7 nucleotide receptor in a mouse microglial cell line. FEBS Lett 581: 3019–3026.
21. Ryu JK, McLarnon JG (2008) Block of purinergic P2X(7) receptor is neuroprotective in an animal model of Alzheimer's disease. Neuroreport 19: 1715–1719.
22. Wang X, Arcuino G, Takano T, Lin J, Peng WG, et al. (2004) P2X7 receptor inhibition improves recovery after spinal cord injury. Nat Med 10: 821–827.
23. Takenouchi T, Sekiyama K, Sekigawa A, Fujita M, Waragai M, et al. (2010) P2X7 receptor signaling pathway as a therapeutic target for neurodegenerative diseases. Arch Immunol Ther Exp (Warsz) 58: 91–96.
24. Bolognesi ML, Ai Tran HN, Staderini M, Monaco A, López-Cobeñas A, et al. (2010) Discovery of a class of diketopiperazines as antiprion compounds. ChemMedChem 5: 1324–1334.
25. Caughey B, Race RE (1992) Potent inhibition of scrapie-associated PrP accumulation by congo red. J Neurochem 59: 768–771.
26. Gilch S, Winklhofer K, Groschup M, Nunziante M, Lucassen R, et al. (2001) Intracellular re-routing of prion protein prevents propagation of PrP(Sc) and delays onset of prion disease. EMBO J 20: 3957–3966.
27. Caughey B, Raymond L, Raymond G, Maxson L, Silveira J, et al. (2003) Inhibition of protease-resistant prion protein accumulation in vitro by curcumin. J Virol 77: 5499–5502.
28. Shimizu Y, Kaku-Ushiki Y, Iwamaru Y, Muramoto T, Kitamoto T, et al. (2010) A novel anti-prion protein monoclonal antibody and its single-chain fragment variable derivative with ability to inhibit abnormal prion protein accumulation in cultured cells. Microbiol Immunol 54: 112–121.
29. Iwamaru Y, Shimizu Y, Imamura M, Murayama Y, Endo R, et al. (2008) Lactoferrin induces cell surface retention of prion protein and inhibits prion accumulation. J Neurochem 107: 636–646.
30. Iwamaru Y, Takenouchi T, Ogihara K, Hoshino M, Takata M, et al. (2007) Microglial cell line established from prion protein-overexpressing mice is susceptible to various murine prion strains. J Virol 81: 1524–1527.
31. Nagaoka K, Yoshioka M, Shimozaki N, Yamamura T, Murayama Y, et al. (2010) Sensitive detection of scrapie prion protein in soil. Biochem Biophys Res Commun 397: 626–630.
32. Sakaguchi S, Katamine S, Shigematsu K, Nakatani A, Moriuchi R, et al. (1995) Accumulation of proteinase K-resistant prion protein (PrP) is restricted by the expression level of normal PrP in mice inoculated with a mouse-adapted strain of the Creutzfeldt-Jakob disease agent. J Virol 69: 7586–7592.
33. Daude N, Marella M, Chabry J (2003) Specific inhibition of pathological prion protein accumulation by small interfering RNAs. J Cell Sci 116: 2775–2779.
34. Caughey B, Raymond GJ (1991) The scrapie-associated form of PrP is made from a cell surface precursor that is both protease- and phospholipase-sensitive. J Biol Chem 266: 18217–18223.
35. Borchelt DR, Taraboulos A, Prusiner SB (1992) Evidence for synthesis of scrapie prion proteins in the endocytic pathway. J Biol Chem 267: 16188–16199.
36. Marijanovic Z, Caputo A, Campana V, Zurzolo C (2009) Identification of an intracellular site of prion conversion. PLoS Pathog 5: e1000426.
37. Goold R, Rabbanian S, Sutton L, Andre R, Arora P, et al. (2011) Rapid cell-surface prion protein conversion revealed using a novel cell system. Nat Commun 2: 281.
38. Yamasaki T, Suzuki A, Shimizu T, Watarai M, Hasebe R, et al. (2012) Characterization of intracellular localization of PrP(Sc) in prion-infected cells using a mAb that recognizes the region consisting of aa 119–127 of mouse PrP. J Gen Virol 93: 668–680.
39. Rambold AS, Miesbauer M, Olschewski D, Seidel R, Riemer C, et al. (2008) Green tea extracts interfere with the stress-protective activity of PrP and the formation of PrP. J Neurochem 107: 218–229.
40. Shyng SL, Lehmann S, Moulder KL, Harris DA (1995) Sulfated glycans stimulate endocytosis of the cellular isoform of the prion protein, PrPC, in cultured cells. J Biol Chem 270: 30221–30229.
41. Murayama Y, Yoshioka M, Yokoyama T, Iwamaru Y, Imamura M, et al. (2007) Efficient in vitro amplification of a mouse-adapted scrapie prion protein. Neurosci Lett 413: 270–273.
42. Jeffrey M, Halliday W, Bell J, Johnston A, MacLeod N, et al. (2000) Synapse loss associated with abnormal PrP precedes neuronal degeneration in the scrapie-infected murine hippocampus. Neuropathol Appl Neurobiol 26: 41–54.
43. Cunningham C, Deacon R, Wells H, Boche D, Waters S, et al. (2003) Synaptic changes characterize early behavioural signs in the ME7 model of murine prion disease. Eur J Neurosci 17: 2147–2155.
44. Kordek R, Hainfellner J, Liberski P, Budka H (1999) Deposition of the prion protein (PrP) during the evolution of experimental Creutzfeldt-Jakob disease. Acta Neuropathol 98: 597–602.
45. Schultz J, Schwarz A, Neidhold S, Burwinkel M, Riemer C, et al. (2004) Role of interleukin-1 in prion disease-associated astrocyte activation. Am J Pathol 165: 671–678.
46. Brown D (2001) Microglia and prion disease. Microsc Res Tech 54: 71–80.
47. Taraboulos A, Raeber AJ, Borchelt DR, Serban D, Prusiner SB (1992) Synthesis and trafficking of prion proteins in cultured cells. Mol Biol Cell 3: 851–863.
48. Quaglio E, Chiesa R, Harris D (2001) Copper converts the cellular prion protein into a protease-resistant species that is distinct from the scrapie isoform. J Biol Chem 276: 11432–11438.
49. Compton SJ, Jones CG (1985) Mechanism of dye response and interference in the Bradford protein assay. Anal Biochem 151: 369–374.
50. Heiseke A, Aguib Y, Riemer C, Baier M, Schätzl H (2009) Lithium induces clearance of protease resistant prion protein in prion-infected cells by induction of autophagy. J Neurochem 109: 25–34.
51. Kang SW, Rane NS, Kim SJ, Garrison JL, Taunton J, et al. (2006) Substrate-specific translocational attenuation during ER stress defines a pre-emptive quality control pathway. Cell 127: 999–1013.
52. Cabral GA, Harmon KN, Carlisle SJ (2001) Cannabinoid-mediated inhibition of inducible nitric oxide production by rat microglial cells: evidence for CB1 receptor participation. Adv Exp Med Biol 493: 207–214.
53. Marsicano G, Goodenough S, Monory K, Hermann H, Eder M, et al. (2003) CB1 cannabinoid receptors and on-demand defense against excitotoxicity. Science 302: 84–88.
54. Khaspekov LG, Brenz Verca MS, Frumkina LE, Hermann H, Marsicano G, et al. (2004) Involvement of brain-derived neurotrophic factor in cannabinoid receptor-dependent protection against excitotoxicity. Eur J Neurosci 19: 1691–1698.
55. Dirikoc S, Priola S, Marella M, Zsürger N, Chabry J (2007) Nonpsychoactive cannabidiol prevents prion accumulation and protects neurons against prion toxicity. J Neurosci 27: 9537–9544.
56. Brown AR, Webb J, Rebus S, Walker R, Williams A, et al. (2003) Inducible cytokine gene expression in the brain in the ME7/CV mouse model of scrapie is highly restricted, is at a strikingly low level relative to the degree of gliosis and occurs only late in disease. J Gen Virol 84: 2605–2611.
57. Tribouillard-Tanvier D, Striebel J, Peterson K, Chesebro B (2009) Analysis of protein levels of 24 cytokines in scrapie agent-infected brain and glial cell cultures from mice differing in prion protein expression levels. J Virol 83: 11244–11253.
58. Walsh D, Betmouni S, Perry V (2001) Absence of detectable IL-1beta production in murine prion disease: a model of chronic neurodegeneration. J Neuropathol Exp Neurol 60: 173–182.
59. Boche D, Cunningham C, Docagne F, Scott H, Perry V (2006) TGFbeta1 regulates the inflammatory response during chronic neurodegeneration. Neurobiol Dis 22: 638–650.
60. Depino AM, Earl C, Kaczmarczyk E, Ferrari C, Besedovsky H, et al. (2003) Microglial activation with atypical proinflammatory cytokine expression in a rat model of Parkinson's disease. Eur J Neurosci 18: 2731–2742.
61. Hracskó Z, Baranyi M, Csölle C, Gölöncsér F, Madarász E, et al. (2011) Lack of neuroprotection in the absence of P2X7 receptors in toxin-induced animal models of Parkinson's disease. Mol Neurodegener 6: 28.
62. Remy M, Thaler S, Schumann RG, May CA, Fiedorowicz M, et al. (2008) An in vivo evaluation of Brilliant Blue G in animals and humans. Br J Ophthalmol 92: 1142–1147.
63. Iriyama A, Kadonosono K, Tamaki Y, Yanagi Y (2012) Effect of Brilliant Blue G on the retinal ganglion cells of rats. Retina 32: 613–616.

RESEARCH PAPER

Prion 7:2, 1–7; March/April 2013; © 2013 Landes Bioscience

Comparison of the local structural stabilities of mammalian prion protein (PrP) by fragment molecular orbital calculations

Koji Hasegawa,[1] Shirou Mohri[2] and Takashi Yokoyama[2,*]

[1]AdvanceSoft Corporation; Tokyo, Japan; [2]Prion Disease Research Center; National Institute of Animal Health; Ibaraki, Japan

Keywords: prion, BSE, species barrier, FMO, structure

Abbreviations: BSE, bovine spongiform encephalopathy; FMO, fragment molecular orbital; IFIE, interfragment interaction energy; NMR, nuclear magnetic resonance; ΔE^{Int}, internal interaction energy; ΔE^{pair}, pair interaction energy; PCA, principal component analysis; PDB, Protein Data Bank; PrP, prion protein; PrP^{C}, cellular PrP; PrP^{Sc}, pathogenic isoform of PrP; vCJD, variant Creutzfeldt-Jakob disease

Bovine spongiform encephalopathy (BSE), a member of the prion diseases, is a fatal neurodegenerative disorder suspected to be caused by a malfunction of prion protein (PrP). Although BSE prions have been reported to be transmitted to a wide range of animal species, dogs and hamsters are known to be BSE-resistant animals. Analysis of canine and hamster PrP could elucidate the molecular mechanisms supporting the species barriers to BSE prion transmission. The structural stability of six mammalian PrPs, including human, cattle, mouse, hamster, dog and cat, was analyzed. We then evaluated intramolecular interactions in PrP by fragment molecular orbital (FMO) calculations. Despite similar backbone structures, the PrP side-chain orientations differed among the animal species examined. The pair interaction energies between secondary structural elements in the PrPs varied considerably, indicating that the local structural stabilities of PrP varied among the different animal species. Principal component analysis (PCA) demonstrated that different local structural stability exists in bovine PrP compared with the PrP of other animal species examined. The results of the present study suggest that differences in local structural stabilities between canine and bovine PrP link diversity in susceptibility to BSE prion infection.

Introduction

Bovine spongiform encephalopathy (BSE), a member of the prion diseases, is a fatal neurodegenerative disorder caused by structural conversion of cellular prion protein (PrP^{C}) into its pathogenic isoform (PrP^{Sc}).[1] However, little is known about the mechanism of this conversion. The *Prnp* gene is highly conserved among many mammalian species and PrP^{C} shows a high degree of homology among mammals, accounting for the ease of cross-species transmission of prion diseases. Several amino acids have been identified as critical for interspecies prion transmission; amino acid substitutions of these critical residues create a species barrier, resulting in diminishment or complete abolition of the efficiency of prion transmission.[2]

A wide range of host species are affected by BSE prions. Experimentally, BSE has been transmitted to mice,[3] sheep, goats,[4] minks,[5] marmosets,[6] macaques[7] and lemurs.[8] In nature, BSE has been transmitted to cattle,[9] several zoo ruminants[10] and domestic and wild cats.[11] Furthermore, BSE has been transmitted to humans via cattle, causing variant Creutzfeldt-Jakob disease (vCJD).[12] On the other hand, several species have been observed to be resistant to BSE infection. Although, no experimental result was reported regarding BSE-challenged dog. While cats were reported to develop feline spongiform encephalopathy, dogs did not appear to be affected by BSE, even after they were fed similarly infected pet food.[13] In addition, typical BSE prions were not transmitted to hamsters at primary passage.[14] Analysis of canine and hamster PrP^{C} could elucidate the molecular mechanisms accounting for the species barrier to BSE prion transmission in these species.

The three-dimensional structure of PrP^{Sc} cannot be determined directly because PrP^{Sc} is insoluble in aqueous solution and has a strong tendency to form fibrils and amorphous aggregates. It has reported that the negative charge of polyoxometalates determines the quaternary structure of PrP^{Sc} fibrils.[15] However, little is currently known about the PrP^{Sc} structures. Nuclear magnetic resonance (NMR) spectroscopy and X-ray crystallography have revealed that the three-dimensional structure of the C-terminal globular domains of PrP^{C} showed similarities among the various mammalian species examined.[16-20] It has reported that β2-α2

*Correspondence to: Takashi Yokoyama; Email: tyoko@affrc.go.jp
Submitted: 10/22/12; Revised: 11/27/12; Accepted: 12/04/12
http://dx.doi.org/10.4161/pri.23122

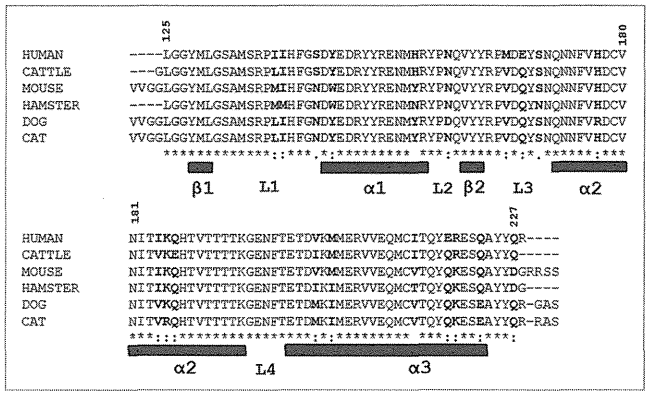

Figure 1. Amino acid sequences of C-terminal region of six mammalian prion proteins (PrPs). The six mammalian PrP sequences were compared. The bold residues are not conserved among the 6 PrPs. The residue numbering for all PrP was aligned with that for human PrP. The secondary structural element information was shown as α for α-helix, β for β-strand and L for loop or coil region.

loop has an important role in intermolecular interactions and it may be a key for PrP aggregation.[21] Still, no critical conformational differences have been identified that are linked to species barriers to prion transmission. An alternate approach is necessary to reveal the structural differences and/or differences in structural stability of PrP^C that exist among the different species.

The ab initio fragment molecular orbital (FMO) calculation is a powerful tool for quantum chemical analysis of intramolecular interactions in proteins and has been utilized to analyze protein-ligand binding affinities[22,23] and protein stabilities.[24-26] Intramolecular interactions between residues play a key role in the structural stability of proteins.[27] The intra- and inter-molecular interactions of mouse PrP models with explicit water has been examined using the FMO-RIMP2 method.[28] Using the FMO calculations, we previously demonstrated that the local structural stability of the E200K mutant of PrP was altered vis à vis that of the wild-type PrP. The instability of the E200K mutant structure is thought to be a trigger for conversion to PrP^{Sc}.[24]

In this study, we compared the intramolecular interactions of six mammalian PrPs ab initio to identify their structural differences, which were not detected by classical methods of structural determination. A clarification of the differences in intramolecular interactions between BSE-susceptible and BSE-resistant hosts may facilitate elucidation of the molecular mechanisms of species barriers to BSE prion transmission. Our calculations showed that canine and bovine PrP differ markedly in their local structural stabilities, providing a possible rationale for why canines and hamsters were resist to BSE infection.

Results

Structural comparison of PrP. The NMR structures of six mammalian PrPs were compared. Their amino acid sequences and secondary structures are shown in **Figure 1**. As reported previously,[16-20] the PrP backbone structures highly resemble one another (**Fig. 2A**). However, the orientation of PrP side chains is different, both on the outer surface and in the internal region (**Fig. 2B**), suggesting that the PrPs of all six animal species show differing intermolecular interactions and/or local structural stabilities.

FMO analysis of intramolecular interactions of PrP. To assess the intramolecular interactions of PrP, an FMO calculation was performed. The values of internal interaction energies (ΔE^{Int}) of nine secondary structural elements were negative, indicating the absence of clear differences among the animal species (**Table S1**). The values of the interfragment interaction energies (IFIEs) of residue pairs were negative or positive, denoting that the pairs were structurally stable or unstable, respectively. Since ΔE^{Int} is generated by summation of all of the IFIEs between the residues belonging to same element, this result suggests that each secondary element is structurally stable and primarily contributes to the similarity in backbone structure among the species. To compare the intramolecular interaction between secondary structural elements, we calculated the energies of 36 pair interactions (**Table 1**). As with IFIE and ΔE^{Int}, the pair interaction energy (ΔE^{Pair}) values were negative or positive, denoting that the pairs were structurally stable or unstable, respectively. It should be noted here that the interaction energies of ΔE^{Int} and ΔE^{Pair} provides information on local structural stabilities for the secondary structure elements of PrP but these energies are enthalpic contributions but not local folding free energies. Although partial unfolding free energies in some specified residues of PrP has been monitored by NMR,[29] present technique could not be used to analyze denaturation status of local elements of PrP. Therefore, there are no experimental data for verifying the obtained FMO calculations. The total ΔE^{Pair} for all species combined was negative, with similar values ranging from -618 to -794 kcal/mol. This result also suggests that the global structure for all PrPs is stable, irrespective of the animal species from which it originates. A maximum and a minimum value of ΔE^{Pair} within each examined animal species is shown in blue and red, respectively, in **Table 1**. As shown in **Table 1**, the ΔE^{Pair} values substantially differed between species on an individual basis. The seven elemental pairs, L1-α1, L1-L2, α1-L4, α1-α3, L3-α3, α2-L4 and α2-α3, showed substantially variability in their interaction energies among the animal species (σ > 20 kcal/mol; **Table 1**). Under mildly acidic pH conditions, the values of the two pairs (L1-α3 and α1-α2) also varied substantially (**Table S2**). These results indicate that the intramolecular interaction networks, specifically, the local structural stabilities, differed considerably among PrP species, despite their similarities in backbone structure. Notably, these differences were primarily caused by differences in minor amino acid residues and/or in structural orientations of side chains.

The interaction between α1 and α2 of BSE-susceptible animals (human, bovine, mouse and cat) ranged from -5 to -18 kcal/mol, whereas that of BSE-resistant animals was -24 kcal/mol (for hamster) and -30 kcal/mol (for dog). Similarly, the interaction between α2 and L4 of BSE-susceptible animals ranged from -48 to -71 kcal/mol and that of BSE-resistant animals was -90 kcal/mol (for dog) and -119 kcal/mol (for hamster). These results indicate that PrP from BSE-resistant animals

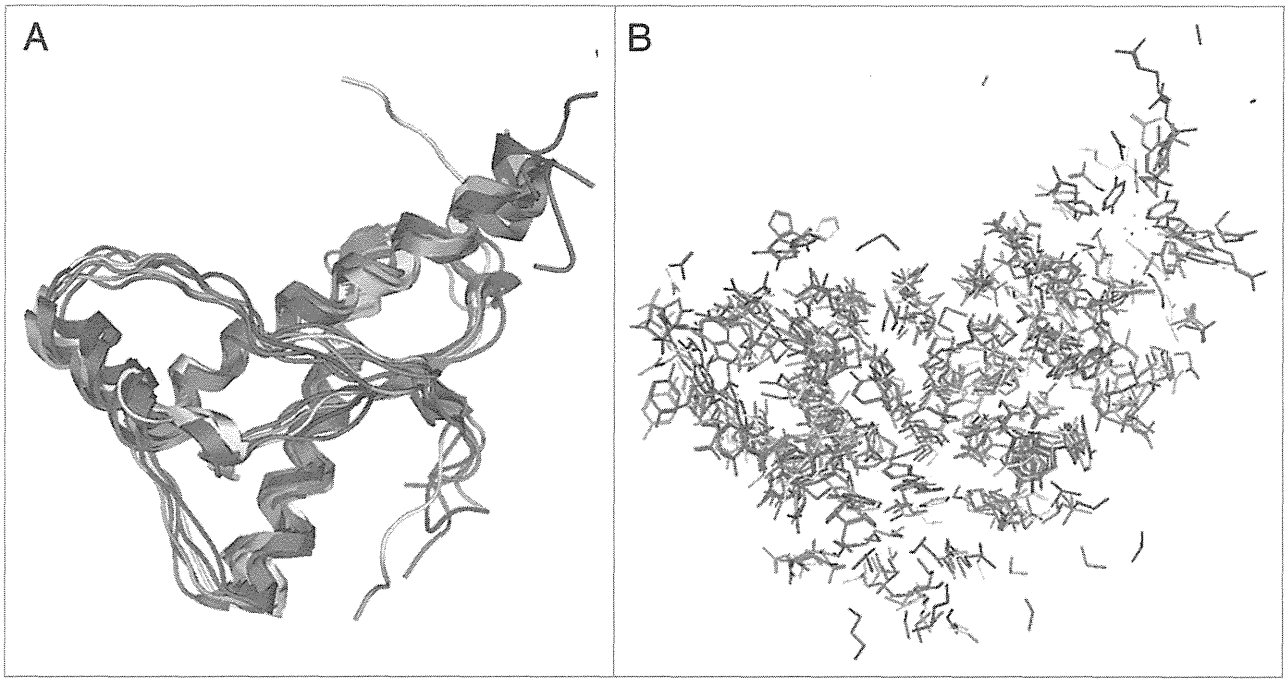

Figure 2. Superposition of the nuclear magnetic resonance (NMR) structures of 6 mammalian PrPs. The structures of backbone (**A**) and side chains (**B**) are illustrated: human (red), bovine (green), mouse (blue), hamster (purple), dog (yellow) and cat (orange).

maintains a relatively stable interaction in α1-α2 and α2-L4 regions (**Table 1**).

PCA for pair interaction energies (ΔE^{Pair}) of PrP. Principal component analysis (PCA) for the ΔE^{Pair} of animal PrP models under neutral and mildly acidic pH conditions was performed to clearly elucidate differences in ΔE^{Pair} values among animal PrPs. The coefficients of the eigenvector for the first principal component showed that ΔE^{Pair} differences were primarily attributable to 4 elemental pairs under neutral pH conditions: L1-α1, α1-L4, α2-L4 and α2-α3; and 6 element pairs under mildly acidic pH conditions L1-α1, L1-L2, α1-α2, α1-L4, α2-L4 and α2-α3 (**Table S2**). **Figure 3** shows the first principal component scores of the ΔE^{Pair} for the six animal PrPs in neutral and mildly acidic pH conditions. The PCA demonstrated that bovine and canine PrPs show markedly different local structural stabilities under neutral pH conditions. The interaction of the α2-α3 pair is significantly weaker in bovine PrP than in PrP of other animals and this difference may explain the peculiar interaction observed in bovine PrP (**Fig. 3**) and this pair energy might be one of the most important factor regarding the BSE sensitivity. The PCA score of the hamster PrP was plotted at a great distance from bovine PrP under mildly acidic pH conditions (**Fig. 3**). Higher principal components in the PCA did not identify any additional useful relationships (data not shown).

Discussion

During the transfer of prions from one species to another, complete failure of transmission or a greatly extended incubation period of affected animals is often encountered. Although the precise mechanisms of this species barrier phenomenon have not been fully elucidated, it is likely to have a biophysical basis in the structural differences between host PrP^{C} and PrP^{Sc} in the inoculum.[1] The conversion from PrP^{C} to PrP^{Sc} may be performed in multiple steps; a heterodimer of PrP^{C} and PrP^{Sc} has been purported to be generated initially.[1] A comparison of structural determinations of PrPs from different species may provide an insight into the susceptibility of a given species to interspecies prion transmission and into the nature of the species barrier.[30]

Although BSE prions have reportedly been transmitted to a wide range of animal species, dogs are known to be BSE-resistant animals.[13] It has also been reported that typical BSE was not transmitted to hamsters at the primary passage.[14] However, an atypical form of BSE known as the L-type BSE, was transmitted to hamsters at the primary passage.[31] This may imply that the resistance in hamsters to BSE prion infection is not absolute or even specific for typical BSE prions. We attempted to compare the structural differences among 6 mammalian PrPs based on their typical BSE susceptibility: four BSE-susceptible animals (cattle, cats, mice and humans) and two BSE-resistant animals (dogs and hamsters).

In this study, we demonstrated that the side-chain orientations of the PrP structures were species specific, irrespective of their similar backbone structures (**Fig. 2**). The geometrical differences in side-chain orientations in PrP caused by point mutations[29,32] or amino acid substitutions[17] have been investigated. These geometrical changes may affect critical intramolecular interactions in PrP. A quantitative evaluation of intramolecular interactions is essential in order to elucidate differences in PrP structural stability.

Table 1. The pair interaction energies (ΔE^{Pair}) of 6 mammalian PrP models under neutral pH condition

	Secondary Structure Element Pairs			Pair Interaction Energies, ΔE/kcal mol^{-1}							
				Human	Cattle	Mouse	Hamster	Dog	Cat	Average[a]	σ[b]
1	β1	–	L1	−29	−32	−34	−15	−24	−20	−26	7
2	β1	–	α1	+0	+0	−0	+0	−0	+0	+0	0
3	β1	–	L2	−1	+0	−2	−0	−0	−1	−1	1
4	β1	–	β2	−26	−22	−23	−16	−25	−35	−25	6
5	β1	–	L3	−29	−32	−17	−26	−25	−13	−24	7
6	β1	–	α2	+0	−2	−22	−5	−14	−2	−7	9
7	β1	–	L4	+0	−0	+0	−0	+0	+0	+0	0
8	β1	–	α3	−1	+2	−8	+2	−5	−4	−2	4
9	L1	–	α1	−123	−105	−133	−120	−84	−65	−105	26*
10	L1	–	L2	−55	−73	−34	−25	−83	−35	−51	23*
11	L1	–	β2	−9	−13	−14	−11	−15	−8	−12	3
12	L1	–	L3	−9	+3	+4	+4	+4	+4	+2	5
13	L1	–	α2	+19	+1	+15	+22	+34	+20	+18	10
14	L1	–	L4	−17	−25	−18	−22	−17	−19	−20	3
15	L1	–	α3	−99	−78	−52	−53	−90	−67	−73	19
16	α1	–	L2	−25	−33	−26	−24	−6	−27	−24	9
17	α1	–	β2	+1	+0	+0	−0	+0	+0	+0	0
18	α1	–	L3	+8	−1	−3	−2	−2	−1	−0	4
19	α1	–	α2	−16	−5	−15	−24	−30	−18	−18	8
20	α1	–	L4	−26	−65	−5	−4	+8	+6	−14	28*
21	α1	–	α3	−8	−11	−79	−22	+6	−49	−27	31*
22	L2	–	β2	−18	−27	−22	−22	−17	−14	−20	5
23	L2	–	L3	−0	+1	+1	+1	−3	+1	−0	2
24	L2	–	α2	−15	−14	−8	−25	−35	−6	−17	11
25	L2	–	L4	−1	−3	−1	−3	+19	+0	+2	8
26	L2	–	α3	−13	−4	−10	−9	+33	−9	−2	17
27	β2	–	L3	−12	−6	−12	−22	−12	−11	−13	5
28	β2	–	α2	−33	−7	−13	−21	−21	+2	−16	12
29	β2	–	L4	+1	+1	+1	+1	+1	+0	+1	0
30	β2	–	α3	−21	−20	−37	−27	−17	−9	−22	9
31	L3	–	α2	−45	−30	−42	−65	−31	−69	−47	17
32	L3	–	L4	+7	−2	−3	−3	−3	−2	−1	4
33	L3	–	α3	+42	−12	−19	−35	−12	−9	−7	26*
34	α2	–	L4	−71	−48	−62	−119	−90	−69	−77	25*
35	α2	–	α3	−89	−28	−56	−101	−160	−119	−92	47*
36	L4	–	α3	−12	−9	−11	−3	+19	+30	+2	18
	Total			−725	−699	−760	−794	−697	−618		

The pair interaction energies were evaluated by summation of the calculated IFIEs between the residues on the element pairs. [a]The average for the values of ΔE^{Pair}. [b]The standard deviations σ for the values of the ΔE^{Pair}. *The varied ΔE^{Pair} among the six mammalian PrP^C; σ ≥ 20 kcal/mol. The blue-marked boxes are the maximum values (i.e., most repulsive interaction) among the PrP species. The red-marked boxes are the minimum values (i.e., most attractive interaction) among the PrP species.

We compared the local structural stabilities of the secondary structural elements of mammalian PrP by FMO calculations. The structural stabilities of the elements were similar among all mammalian species (**Table S1**). However, our calculations show a considerably wide range of ΔE^{Pair} values in the specific local pairs and it indicates that the local structural stabilities varied among different animal species (**Table 1**). Since the magnitude of ΔE^{Pair} is indicative of the strength of the interaction, a negative value of ΔE^{Pair} denotes an attractive interaction (i.e., a structurally stable conformation), whereas a positive value denotes a repulsive interaction (i.e., a structurally unstable conformation). The stable pair regions are expected to be less susceptible to denaturation of structural conformation. These local regions could possess a highly variable internal local protein dynamics properties among the different animal species.

It is believed that the endosomes of scrapie-infected cells, characterized by mildly acidic pH conditions (pH 4.0–6.0), are the sites of PrP^{Sc} accumulation, while the cell surface, characterized by neutral pH conditions (~pH 7), is the site of PrP^C binding to PrP^{Sc}.[33] It has also reported that the endosomal recycling compartment is thought as the site of prion conversion.[34] Our calculations revealed that the local structural stabilities denoted by ΔE^{Pair} in the specific regions are markedly altered under lower pH conditions, an observation that highly depended on the animal species examined (**Table 1 and Table S2**). Local structural stability of PrP varied with changes in pH conditions and no similarities among animal species were observed in association with pH alteration. This suggests that PrP^{Sc} conversion mechanisms differ depending on the animal species.

Our calculations also demonstrated that the total structural stabilities of the PrPs in different species were not directly related to their BSE susceptibilities and/or resistance, suggesting a greater importance for local structure of PrP in the elucidation of PrP denaturation properties. To clarify this difference among

animal species, we performed a PCA. The analysis clearly demonstrated that different structural stabilities exist between dog and cattle under neutral conditions and between hamster and cattle under mildly acidic conditions (**Fig. 3**). This observation suggests that different mechanisms underlie the resistance to BSE infection between dog and hamster. Our analysis showed that bovine PrP possessed markedly different characteristics from other PrPs, consistent with a previous observation that bovine PrP is more highly resistant to urea denaturation than are PrPs of other species.[29]

The peculiar local structural stabilities of bovine PrP was primarily derived by the weaker stability of the α2-α3 interaction. Furthermore, relatively weak interactions of α1-α2 and α2-L4 were observed in BSE-susceptible animals. These results may be explained by the hypothesis that PrP with weak interactions among α1, α2 and α3 sites could be converted to PrP^{Sc} by BSE prion infection. This may also account for the observation that resistance against proteolysis of PrP^{Sc} from BSE was weaker than that against scrapie.[35]

In conclusion, our FMO calculations revealed the different structural stabilities of PrP among different animal species. Cattle PrP has different biophysical characteristics from other mammalian PrPs. The results of this study suggest that differences in local structural stabilities of α1-α2 and α2-L4 of PrP provide a link to the mechanisms of species barriers against BSE prion infection.

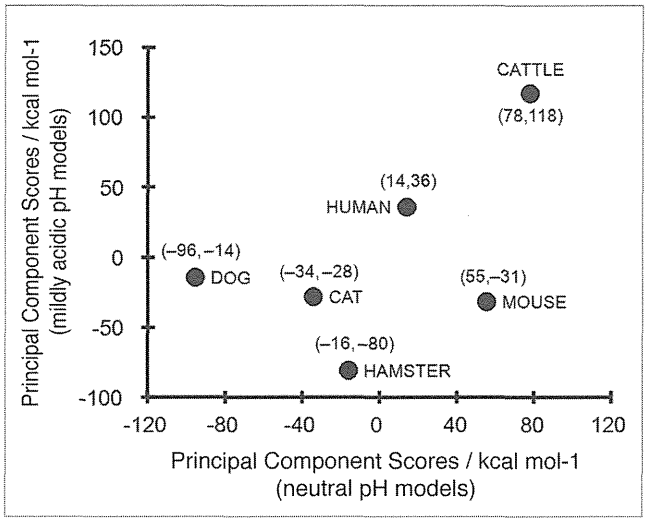

Figure 3. First principal component scores in the principal component analysis (PCA) for the ΔE^{Pair} of mammalian PrP. The scores under neutral (pH 7.0) and mildly acidic (pH 4.5) models were plotted in axes of abscissas and ordinates, respectively. The numerical values in the parenthesis are the scores for neutral pH and mildly acidic pH models, respectively.

Materials and Methods

Structural modeling of PrPs for FMO calculations. Initial atomic coordinates of mammalian PrP for human, cattle, mouse, hamster, dog and cat were extracted from the Protein Data Bank (PDB) structures with the codes 1QM3, 1DWZ, 1XYX, 1B10, 1XYK and 1XYJ, respectively. The residue numbering for all PrP species was identical to that of human PrP. The secondary structures of PrP were defined as follows: three α-helices (α1: 144–156, α2: 172–194 and α3: 200–223), two β-strands (β1: 129–131 and β2: 161–163) and four loop regions (L1: 132–143, L2: 157–160, L3: 164–171 and L4: 195–199) (**Fig. S1**). A multiple sequence alignment for the six PrPs was carried out using ClustalW (1.8.3 WWW Server in DNA Data Bank of Japan, National Institute of Genetics)[36] (**Fig. 1**). The PrP structural models were constructed for the top five conformers deposited in the PDB. For the neutral pH (pH 7.0) model of the PrPs as a cell surface model,[24] we made the following assumptions: (1) lysine, arginine and the N–terminal residues were positively charged; (2) glutamic acid, aspartic acid and the C-terminal residues were negatively charged; and (3) histidines were neutrally protonated at the Nτ atom. All other residues were considered to be neutrally charged. In the mildly acidic (pH 4.5) condition, the protonation states were identical to the pH 7.0, with the exception of histidines, in which the side chains were imidazolium forms and thus positively charged. The proteins in explicit water were modeled by arranging water molecules in a sphere within 16 Å of the protein surface. The geometric optimizations for protein models in water were performed using an AMBER99 force field with constraints of fixed heavy atoms in the whole protein, followed by restricting of the water molecules within 8 Å on the protein (1,489–1,913 molecules) for FMO calculations. Examples of solvated models are shown in **Figure S2**. The generated models were further optimized under constraints of fixed heavy atoms, with the exceptions of N- and C-terminal residues of the proteins. The modeling procedures were performed using MOE (version 2011.10, Chemical Computing Group, Inc.).

FMO calculations. Ab initio FMO calculations were carried out using the ABINIT-MP software (Advance/BioStation ver. 3.3, Advance Soft Corp.) with the RI-MP2 method[37,38] combined with the 6-31G basis set. In the FMO calculation, the protein models were fragmented into single amino acid residues, with the exception of the disulfide-bond residues of Cys176 and Cys214, which were considered a single fragment. The interfragment interaction energy (IFIE) between covalently adjoining residues were evaluated by subtracting the calculated IFIE from an IFIE between methyl groups in an ethylene molecule with a gauche form; this form has an identical C-C bond length with a bond length between a Cα atom and a backbone carbonyl C atom in the residues of the protein structure.[39] An average of the IFIEs was calculated for the top five conformer models. The pair interaction energy ΔE_{PQ}^{Pair} between the elements P and Q was evaluated using the following equation:

$$\Delta E_{PQ}^{Pair} = \sum_{I \in P} \sum_{J \in Q} \Delta E \quad (1)$$

where the ΔE_{IJ} is the IFIE between the I and J fragments in the P and Q elements, respectively. The internal interaction energy ΔE_{P}^{Int} for the element P was calculated using the following equation:

$$\Delta E_{P}^{Int} = \sum_{I \in P} \sum_{J \in P} \Delta E_{IJ} \quad (2)$$

The IFIE for the disulfide bond fragment was considered in the ΔE_{PQ}^{Pair} and ΔE_{P}^{Int} as described previously.[22] A typical run of a PrP model with explicit water took a calculation time of 10 hours on average using four quad-core AMD Opteron 2.5 GHz cluster (16 CPUs).

PCA. The PCA for the ΔE^{Pair} was performed by solving an eigenvalue problem for an actual variance-covariance matrix built from the variances of ΔE^{Pair}. The PCA was carried out using the statistical functions in the Microsoft Excel package (Microsoft Corp.). The principal component score of each animal species for the first principal component was obtained by calculating an inner product of the eigenvector for the first principal component and the vector whose components were the values that were generated by subtracting averaged ΔE^{Pair} over all species from ΔE^{Pair}.

Disclosure of Potential Conflicts of Interest

No potential conflicts of interest were disclosed.

Acknowledgments

The numerical calculations were supported by the Agriculture, Forestry and Fisheries Research Technology Center (AFFRIT). We thank Reiko Takeuchi for her general assistance. This study was supported by a grant-in-aid from the BSE and other Prion Disease Control Projects of the Ministry of Agriculture, Forestry and Fisheries, Japan.

References

1. Prusiner SB. Molecular biology of prion diseases. Science 1991; 252:1515-22; PMID:1675487; http://dx.doi.org/10.1126/science.1675487.
2. Moore RA, Vorberg I, Priola SA. Species barriers in prion diseases--brief review. Arch Virol Suppl 2005; 19:187-202; PMID:16355873.
3. Fraser H, Bruce ME, Chree A, McConnell I, Wells GA. Transmission of bovine spongiform encephalopathy and scrapie to mice. J Gen Virol 1992; 73:1891-7; PMID:1645134; http://dx.doi.org/10.1099/0022-1317-73-8-1891.
4. Foster JD, Hope J, Fraser H. Transmission of bovine spongiform encephalopathy to sheep and goats. Vet Rec 1993; 133:339-41; PMID:8236676; http://dx.doi.org/10.1136/vr.133.14.339.
5. Robinson MM, Hadlow WJ, Huff TP, Wells GA, Dawson M, Marsh RF, et al. Experimental infection of mink with bovine spongiform encephalopathy. J Gen Virol 1994; 75:2151-5; PMID:8077914; http://dx.doi.org/10.1099/0022-1317-75-9-2151.
6. Baker HF, Ridley RM, Wells GA, Ironside JW. Prion protein immunohistochemical staining in the brains of monkeys with transmissible spongiform encephalopathy. Neuropathol Appl Neurobiol 1998; 24:476-86; PMID:9888158; http://dx.doi.org/10.1046/j.1365-2990.1998.00142.x.
7. Lasmézas CI, Deslys JP, Demaimay R, Adjou KT, Lamoury F, Dormont D, et al. BSE transmission to macaques. Nature 1996; 381:743-4; PMID:8657276; http://dx.doi.org/10.1038/381743a0.
8. Bons N, Mestre-Frances N, Belli P, Cathala F, Gajdusek DC, Brown P. Natural and experimental oral infection of nonhuman primates by bovine spongiform encephalopathy agents. Proc Natl Acad Sci U S A 1999; 96:4046-51; PMID:10097160; http://dx.doi.org/10.1073/pnas.96.7.4046.
9. Wells GAH, Wilesmith JW. The neuropathology and epidemiology of bovine spongiform encephalopathy. Brain Pathol 1995; 5:91-103; PMID:7767494; http://dx.doi.org/10.1111/j.1750-3639.1995.tb00580.x.
10. Kirkwood JK, Cunningham AA. Epidemiological observations on spongiform encephalopathies in captive wild animals in the British Isles. Vet Rec 1994; 135:296-303; PMID:7817514; http://dx.doi.org/10.1136/vr.135.13.296.
11. Hewicker-Trautwein M, Bradley R. Portrait of transmissible feline spongiform encephalopathy. In: Hornlimann B, Riesner D, Kretzschmar H, eds. Prions in humans and animals. Berlin: Walter de Gruyter 2006:271-4.
12. Collinge J, Sidle KC, Meads J, Ironside J, Hill AF. Molecular analysis of prion strain variation and the aetiology of 'new variant' CJD. Nature 1996; 383:685-90; PMID:8878476; http://dx.doi.org/10.1038/383685a0.
13. Kirkwood JK, Cunningham AA. Epidemiological observations on spongiform encephalopathies in captive wild animals in the British Isles. Vet Rec 1994; 135:296-303; PMID:7817514; http://dx.doi.org/10.1136/vr.135.13.296.
14. Yokoyama T, Masujin K, Iwamaru Y, Imamura M, Mohri S. Alteration of the biological and biochemical characteristics of bovine spongiform encephalopathy prions during interspecies transmission in transgenic mice models. J Gen Virol 2009; 90:261-8; PMID:19088297; http://dx.doi.org/10.1099/vir.0.004754-0.
15. Wille H, Shanmugam M, Murugesu M, Ollesch J, Stubbs G, Long JR, et al. Surface charge of polyoxometalates modulates polymerization of the scrapie prion protein. Proc Natl Acad Sci U S A 2009; 106:3740-5; PMID:19223590; http://dx.doi.org/10.1073/pnas.0812770106.
16. Zahn R, Liu A, Lührs T, Riek R, von Schroetter C, López García F, et al. NMR solution structure of the human prion protein. Proc Natl Acad Sci U S A 2000; 97:145-50; PMID:10618385; http://dx.doi.org/10.1073/pnas.97.1.145.
17. Gossert AD, Bonjour S, Lysek DA, Fiorito F, Wüthrich K. Prion protein NMR structures of elk and of mouse/elk hybrids. Proc Natl Acad Sci U S A 2005; 102:646-50; PMID:15647363; http://dx.doi.org/10.1073/pnas.0409008102.
18. López Garcia F, Zahn R, Riek R, Wüthrich K. NMR structure of the bovine prion protein. Proc Natl Acad Sci U S A 2000; 97:8334-9; PMID:10899999; http://dx.doi.org/10.1073/pnas.97.15.8334.
19. Lysek DA, Schorn C, Nivon LG, Esteve-Moya V, Christen B, Calzolai L, et al. Prion protein NMR structures of cats, dogs, pigs, and sheep. Proc Natl Acad Sci U S A 2005; 102:640-5; PMID:15647367; http://dx.doi.org/10.1073/pnas.0408937102.
20. Liu H, Farr-Jones S, Ulyanov NB, Llinas M, Marqusee S, Groth D, et al. Solution structure of Syrian hamster prion protein rPrP(90-231). Biochemistry 1999; 38:5362-77; PMID:10220323; http://dx.doi.org/10.1021/bi982878x.
21. Sigurdson CJ, Joshi-Barr S, Bett C, Winson O, Manco G, Schwarz P, et al. Spongiform encephalopathy in transgenic mice expressing a point mutation in the β2-α2 loop of the prion protein. J Neurosci 2011; 31:13840-7; PMID:21957246; http://dx.doi.org/10.1523/JNEUROSCI.3504-11.2011.
22. Fukuzawa K, Mochizuki Y, Tanaka S, Kitaura K, Nakano T. Molecular interactions between estrogen receptor and its ligand studied by the ab initio fragment molecular orbital method. J Phys Chem B 2006; 110:16102-10; PMID:16898767; http://dx.doi.org/10.1021/jp060770i.
23. Sawada T, Hashimoto T, Nakano H, Suzuki T, Suzuki Y, Kawaoka Y, et al. Influenza viral hemagglutinin complicated shape is advantageous to its binding affinity for sialosaccharide receptor. Biochem Biophys Res Commun 2007; 355:6-9; PMID:17292854; http://dx.doi.org/10.1016/j.bbrc.2006.12.239.
24. Hasegawa K, Mohri S, Yokoyama T. Fragment molecular orbital calculations reveal that the E200K mutation markedly alters local structural stability in the human prion protein. Prion 2010; 4:38-44; PMID:20139714; http://dx.doi.org/10.4161/pri.4.1.10890.
25. Ishikawa T, Ishikura T, Kuwata K. Theoretical study of the prion protein based on the fragment molecular orbital method. J Comput Chem 2009; 30:2594-601; PMID:19408278; http://dx.doi.org/10.1002/jcc.21265.
26. Fukuzawa K, Komeiji Y, Mochizuki Y, Kato A, Nakano T, Tanaka S. Intra- and intermolecular interactions between cyclic-AMP receptor protein and DNA: ab initio fragment molecular orbital study. J Comput Chem 2006; 27:948-60; PMID:16586530; http://dx.doi.org/10.1002/jcc.20399.
27. Stites WE. Protein-protein Interactions: Interface Structure, Binding Thermodynamics, and Mutational Analysis. Chem Rev 1997; 97:1233-50; PMID:11851449; http://dx.doi.org/10.1021/cr960387h.
28. Ishikawa T, Kuwata K. Interaction analysis of the native structure of prion protein with quantum chemical calculations. J Chem Theory Comput 2010; 6:538-47; http://dx.doi.org/10.1021/ct900456v.
29. Julien O, Chatterjee S, Bjorndahl TC, Sweeting B, Acharya S, Semenchenko V, et al. Relative and regional stabilities of the hamster, mouse, rabbit, and bovine prion proteins toward urea unfolding assessed by nuclear magnetic resonance and circular dichroism spectroscopies. Biochemistry 2011; 50:7536-45; PMID:21800884; http://dx.doi.org/10.1021/bi200731e.
30. Schwarzinger S, Willbold D, Ziegler J. Structural studies of prion proteins. In: Hornlimann B, Riesner D, Kretzschmar H, eds. Prions in humans and animals. Berlin: Walter de Gruyter 2006:79-94.
31. Shu YJ, Masujin K, Okada H, Iwamaru Y, Imamura M, Matsuura Y, et al. Characterization of Syrian hamster adapted prions derived from L-type and C-type bovine spongiform encephalopathies. Prion 2011; 5:103-8; PMID:21597334; http://dx.doi.org/10.4161/pri.5.2.15847.
32. Calzolai L, Lysek DA, Guntert P, von Schroetter C, Riek R, Zahn R, et al. NMR structures of three single-residue variants of the human prion protein. Proc Natl Acad Sci U S A 2000; 97:8340-5; PMID:10900000; http://dx.doi.org/10.1073/pnas.97.15.8340.
33. Borchelt DR, Taraboulos A, Prusiner SB. Evidence for synthesis of scrapie prion proteins in the endocytic pathway. J Biol Chem 1992; 267:16188-99; PMID:1353761.

34. Marijanovic Z, Caputo A, Campana V, Zurzolo C. Identification of an intracellular site of prion conversion. PLoS Pathog 2009; 5:e1000426; PMID:19424437; http://dx.doi.org/10.1371/journal.ppat.1000426.
35. Kuczius T, Groschup MH. Differences in proteinase K resistance and neuronal deposition of abnormal prion proteins characterize bovine spongiform encephalopathy (BSE) and scrapie strains. Mol Med 1999; 5:406-18; PMID:10415165.
36. Thompson JD, Higgins DG, Gibson TJ. CLUSTAL W: improving the sensitivity of progressive multiple sequence alignment through sequence weighting, position-specific gap penalties and weight matrix choice. Nucleic Acids Res 1994; 22:4673-80; PMID:7984417; http://dx.doi.org/10.1093/nar/22.22.4673.
37. Ten-no S, Iwata S. Three-center expansion of electron repulsion integrals with linear combination of atomic electron distributions. Chem Phys Lett 1995; 240:578-84; http://dx.doi.org/10.1016/0009-2614(95)00564-K.
38. Ten-no S, Iwata S. Multiconfiguration self-consistent field procedure employing linear combination of atomic-electron distributions. J Chem Phys 1996; 105:3604-11; http://dx.doi.org/10.1063/1.472231.
39. Fedorov DG, Kitaura K. Pair interaction energy decomposition analysis. J Comput Chem 2007; 28:222-37; PMID:17109433; http://dx.doi.org/10.1002/jcc.20496.

NOTE *Virology*

Retrospective Analysis of Sheep Scrapie by Western Blotting with Formalin-Fixed Paraffin-Embedded (FFPE) Tissues

Gantsetseg DORJ[1,2], Hiroyuki OKADA[1], Kohtaro MIYAZAWA[1], Kentaro MASUJIN[1], Kumiko KIMURA[3], Shirou MOHRI[1] and Takashi YOKOYAMA[1]*

[1]*Prion Disease Research Center, National Institute of Animal Health, Tsukuba 305-0856, Japan*
[2]*State Central Veterinary Laboratory, Ulaanbaatar 17024, Mongolia*
[3]*Subtropical Disease Research Division, National Institute of Animal Health, Chuzan, Kagoshima 891-0105, Japan*

(Received 29 January 2012/Accepted 18 April 2012/Published online in J-STAGE 15 May 2012)

ABSTRACT. An abnormal isoform of prion protein (PrP^{Sc}) was extracted from formalin-fixed paraffin-embedded (FFPE) tissues from sheep and analyzed by western blotting. PrP^{Sc} immunoreactivity against anti-PrP monoclonal antibody T2, which recognizes discontinuous PrP sequences, differed amongst individual scrapie sheep cases. This may reflect structural differences in PrP^{Sc} that have been formalin-fixed prior to their extraction. This study indicates that western blotting by using FFPE tissues is useful for the retrospective analysis of transmissible spongiform encephalopathies in which only formalin-fixed samples are available and in conducting transmissible spongiform encephalopathies surveillance where freezing system is insufficient.
KEY WORDS: FFPE, prion, PrP^{Sc}, scrapie, WB.

doi: 10.1292/jvms.12-0037; *J. Vet. Med. Sci.* 74(9): 1207–1210, 2012

Transmissible spongiform encephalopathies (TSEs) are neurodegenerative disorders that affect humans and animals. Bovine spongiform encephalopathy (BSE) in cattle, scrapie in sheep and goats, and Creutzfeldt-Jakob disease in humans are examples of disorders included in this category [15]. Abnormal isoforms of prion proteins (PrP^{Sc}) are major components of pathogenesis [15], and the detection of PrP^{Sc} is the key for TSE diagnosis. Western blotting (WB) and immunohistochemistry (IHC) are routinely used as confirmatory tests. Although WB is a convenient biochemical technique for the detection of PrP^{Sc}, it is not always used because it requires frozen or fresh tissue samples.

Scrapie is caused by many different prion strains, which are characterized by their incubation periods and neuropathology in inbred mice [5]. Strain-specific properties are attributed to the different conformations of PrP^{Sc} [1, 2, 13, 18]. The molecular profiles of PrP^{Sc} in WB, including the glycoprofiles and molecular weights of proteinase-K (PK)-digested PrP^{Sc}(PrPcore), are used for the classification of prion strains [3]. As such, it is known that the PrP^{Sc} of BSE and that of scrapie in sheep can be distinguished using WB [14].

In Mongolia, sheep and goats are the major livestock, with hide, skin, cashmere, and meat exports increasing every year. Because there have been no outbreaks of scrapie in Mongolia to date, it is of crucial importance that Mongolian sheep and goats are confirmed negligible of scrapie infection through consistent surveillance. Unfortunately, it is often difficult to collect and transport frozen brain tissues to laboratories for surveillance, which is also an issue experienced by BSE-affected countries. This is primarily because of geography, with Mongolia being a vast extent of land that includes both deserts to mountainous regions that can be subject to harsh climatic conditions. Nonetheless, pathological examinations are routinely used for the diagnosis of contagious diseases, including rabies and listeriosis.

It has been reported that PrP^{Sc} extracted from formalin-fixed paraffin-embedded (FFPE) tissues can be detected by WB [12]. Because this technique could enable better TSE surveillance, we tested its usefulness on tissues from sheep scrapie cases for which frozen tissues were unavailable. We have demonstrated that WB analysis by using FFPE will be useful for retrospective analysis of transmissible spongiform encephalopathies.

Brain samples containing scrapie Chandler [7], 79A (TSE Resource Center, Compton, UK), Kanagawa [10], and mouse–adapted BSE [6] affected wild-type mice (ICR) were used. Samples were either stored at −80°C for biochemical analysis, or fixed in 10% buffered formalin solution and embedded in paraffin for histopathological and immunohistochemical examination. Fixed tissues were treated with 98% formic acid for 60 min to reduce their infectivity [17] prior to embedding. Furthermore, 4 FFPE tissues of natural sheep scrapie cases were also examined (Table 1).

For the purification of PrP^{Sc} from frozen tissues, brains were homogenized in a buffer containing 100 mM NaCl and 50 mM Tris-HCl (pH 7.6). The homogenate was mixed with an equal volume of detergent buffer containing 4% Zwittergent 3–14, 1% sarkosyl, 100 mM NaCl, and 50 mM Tris-HCl (pH 7.6) and then incubated with 0.25 mg collagenase. The homogenate was then incubated with 40 μg/m*l* of PK at

*CORRESPONDENCE TO: YOKOYAMA T., Prion Disease Research Center, National Institute of Animal Health, 3-1-5 Kannondai, Tsukuba, Ibaraki 305-0856, Japan.
e-mail: tyoko@affrc.go.jp

Table 1. PrP^{Sc} detection from FFPE tissues of scrapie sheep

No.	Sheep breed	Year	Scrapie diagnosis		PrP^{Sc} detection from FFPE tissues		Remarks
			WB	IHC	mAb T2	mAb SAF84	
1	Corriedale	1991	ND[a)]	+	±	++	Field case at Fukushima, Fig.2, lane 1
2	Suffolk	1994	ND	+	±	+++	Field case at Hokkaido-1, Fig. 2, lane 2
3	Suffolk	1994	ND	+	±	+++	Field case at Hokkaido-2, Fig. 2, lane 3
4	Suffolk	1999	ND	+	++	+++	Field case at Tokyo, Fig.2, lane 4

a) Not done (no frozen sample was available).

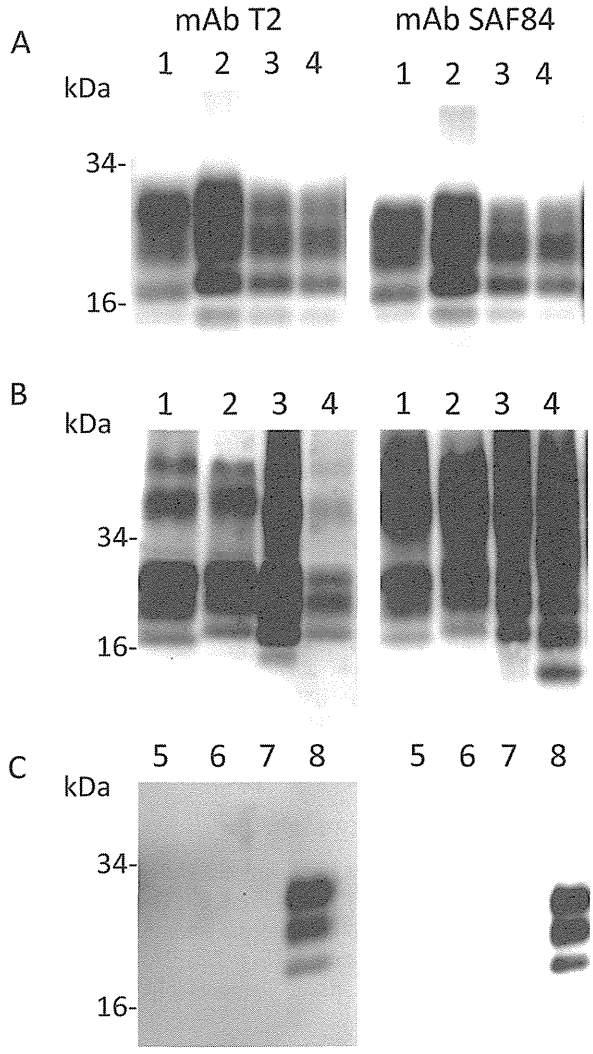

Fig. 1. PrP^{Sc} analysis of frozen tissues (A) and FFPE tissues (B) by using western blotting A. PrP^{Sc} extracted from frozen tissues was detected using mAbs T2 (left panel) and SAF84 (right panel). B. PrP^{Sc} extracted from FFPE tissue was detected using mAbs T2 and SAF84. Lane 1, mouse-adapted BSE-affected ICR mice; lane 2, Scrapie Kanagawa strain-affected ICR mice; lane 3, mouse-adapted scrapie 79A strain-affected ICR mice. This sample was examined without formic acid treatment. Lane 4, mouse–adapted scrapie Chandler strain-affected ICR mice. C. Lanes 5–7, FFPE tissues from normal mouse brains. Lane 8, PrP^{Sc} from mouse–adapted scrapie (frozen tissue).

37°C for 30 min. PK digestion was terminated using 2 mM 4-(2-aminoethyl)-benzenesulfonyl fluoride hydrochloride (Pefabloc; Roche Diagnostics). The sample was mixed with 2-butanol:methanol (5:1) and centrifuged at 20,000 × *g* for 10 min. The final pellet was analyzed using WB.

The protocol for PrP^{Sc} extraction from FFPE tissues was followed as reported previously [8] with minor modifications. Briefly, a section from each FFPE tissue block (PET block) was collected into a 1.5-m*l* microcentrifuge tube. To each tube, 150 μl of buffer (50 mM Tris, 1 mM EDTA, 0.5% Tween 20, pH 7.5) was added. The tube was incubated at 100°C for 10 min and was then immediately frozen with cold ethanol for 5 min. This process was repeated once, and the tubes were then incubated for additional 10 min at 100°C. The sample was then immediately centrifuged at 20,000 × *g* for 15 min to separate the paraffin from the buffer. The tissue pellets and aqueous layer were transferred to another tube, and 150 μl of detergent buffer containing 4% Zwittergent 3–14, 1% sarkosyl, 100 mM NaCl, and 50 mM Tris-HCl (pH 7.6) was added. The pellet was dispersed by sonication and mechanical shearing by using a 27-gauge needle. The sample was then mixed with PK to a final concentration of 50 μg/m*l* and incubated at 37°C for 30 min. Digestion was stopped by adding 1 mM of Pefabloc. The sample was mixed with 2-butanol:methanol (5:1) and centrifuged at 20,000 × *g* for 10 min. The final pellet was analyzed using WB as described previously [9]. The PrP signal was detected using either anti-PrP mAb SAF84 (SPI-Bio, Montigny le Bretonneux, France) and T2 [16], which react against epitopes 160–170 of human PrP sequences and 163–168 of murine PrP sequences, respectively.

WB analysis of PrP^{Sc} from frozen tissues of wild-type mice is shown in Fig. 1A, and the 2 mAbs showed a typical PrP^{Sc} banding pattern. PrP^{Sc} was detected in all the FFPE tissue samples that were examined using both mAbs (Fig. 1B). The molecular weight of PrP^{Sc} from BSE-affected wild-type mice was lower than that of samples from scrapie (Fig. 1, lane 1). Although the molecular weights of PrPcore from FFPE tissues were consistent with those of PrP^{Sc} from frozen tissues for both T2 and SAF84, the glycoform profile of PrPcore from FFPE tissues was resembled but not consistent with that of frozen tissues (Fig. 1A). A ~14 kDa PrP^{Sc} fragment was detected using mAb SAF84 in the FFPE tissue of Chandler-affected mice (Fig.1B, lane 4), but this truncated fragment was not detected during the analysis of frozen tissues (Fig. 1A, lane 4). Formalin fixation influenced PK

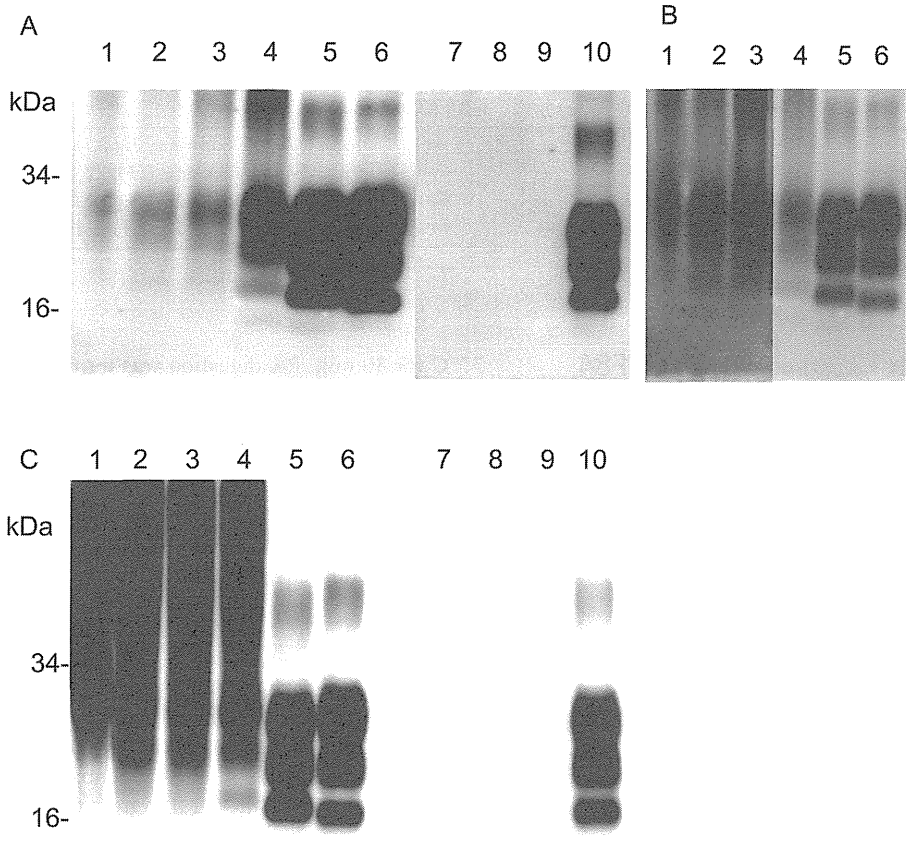

Fig. 2. Comparison of immunoreactivity of PrP^{Sc} extracted from FFPE tissue of natural scrapie A. PrP^{Sc} extracted from FFPE tissue of natural scrapie was detected using mAb T2. B. The same membrane was exposed longer time to visualize the unglycosylated PrP^{Sc} band. C. The same sample was analyzed using mAb SAF84. Lane 1, field scrapie case of 1991; lanes 2 and 3, field scrapie case of 1994; lane 4, field scrapie case of 1999; lanes 5 and 10, PrP^{Sc} extracted from typical scrapie sheep brain (frozen tissue); lane 6, PrP^{Sc} from BSE-affected cattle brain (frozen tissue); lanes 7–9, TSE-negative sheep brain samples.

digestion of PrP^{Sc} and producing some PrP^{Sc} in a partially digested truncated form. Furthermore, strong signals of ~40 kDa were detected for all the PrP^{Sc} from the FFPE tissues that were examined using SAF84 (Fig. 1B). Formalin fixation induces alkylation of amino residues and cross-linking between bio-molecules. Though the precise mechanisms are obscure, these phenomena may cause by this cross-linking. No PrP signals, either low- or high-molecular weight, were detected in TSE-negative FFPE tissue samples (Fig. 1C).

Then, we examined the PrP^{Sc} detection in FFPE tissues from natural sheep scrapie. PrP^{Sc} was extracted from FFPE tissue samples obtained from 2 breeds of sheep having scrapie (Suffolk and Corriedale). These samples were fixed between 1991 and 1999 and stored at room temperature. The PrP^{Sc} signal was clearly detected in 1 sample (Case No. 4), while a weak positive signal was detected in the other 3 samples (Case Nos. 1–3) by using mAb T2 (Table 1, Fig 2A). In contrast, all the examined samples showed a strong positivity for mAb SAF84 (Table 1, Fig. 2C). The molecular weights of the PrPcore from the 4 natural scrapie cases were similar to those of typical scrapie (Fig. 2B). No PrP signal was detected in the FFPE tissue samples obtained from healthy sheep (Fig. 2).

We have shown that PrP^{Sc} can be extracted from FFPE tissues [8, 11]. In this study, we used 2 different mAbs. PrP^{Sc} from FFPE tissues of scrapie sheep have different immunoreactivities against mAb T2, which recognizes discontinuous sequences at PrP163–168 [16]. We concluded that the different immunoreactivities of PrP^{Sc} in FFPE tissues were not associated with the sheep breed or sample storage time but may be potentially associated with their conformational differences. Our results showed the possibility that immunoreactivity of PrP^{Sc} from FFPE tissues might be associated with prion strain diversities in sheep.

The molecular weights of all the PrPcore extracted from FFPE tissues of natural scrapie cases were similar to those of typical scrapie but different from those from BSE (Fig. 2B). This result indicates that these scrapie cases occurred independently of BSE; however, it is important to note that the origin of BSE has not been identified and sheep scrapie has been considered as a candidate of origin. Furthermore, the potential presence of BSE in small ruminants is cautioned, and a BSE case in a goat has been reported [4]. To investigate the relationship between BSE and scrapie, characterization of individual prions is necessary.

This technique could detect PrP^{Sc} from FFPE tissues that were kept more than 10 years. Our study showed that WB analysis by using FFPE will be useful for retrospective analysis in which only formalin-fixed samples are available and in conducting TSE surveillance where freezing system is insufficient.

ACKNOWLEDGMENTS. We thank Yurie Komine, JICA officer, for her kind assistance. We also thank Naoko Tabeta, Naomi Furuya, and Ritsuko Miwa for their technical assistance and Reiko Takeuchi and Junko Yamada for their general assistance. This study was supported by funds for the JICA training course "Veterinary Research Diagnosis" and a BSE control program overseen by the Ministry of Agriculture, Forestry, and Fisheries, Japan. We also thank the staff of the Prion Disease Research Center of the National Institute of Animal Health for their critical comments.

REFERENCES

1. Aguzzi, A. 2004. Understanding the diversity of prions. *Nat. Cell Biol.* **6**: 290–292. [Medline] [CrossRef]
2. Bessen, R. A. and Marsh, R. F. 1992. Biochemical and physical properties of the prion protein from two strains of the transmissible mink encephalopathy agent. *J. Virol.* **66**: 2096–2101. [Medline]
3. Collinge, J., Sidle, K. C., Meads, J., Ironside, J. and Hill, A. F. 1996. Molecular analysis of prion strain variation and the aetiology of 'new variant' CJD. *Nature* **383**: 685–690. [Medline] [CrossRef]
4. Eloit, M., Adjou, K., Coulpier, M., Fontaine, J. J., Hamel, R., Lilin, T., Messiaen, S., Andreoletti, O., Baron, T., Bencsik, A., Biacabe, A. G., Beringue, V., Laude, H., Le Dur, A., Vilotte, J. L., Comoy, E., Deslys, J. P., Grassi, J., Simon, S., Lantier, F. and Sarradin, P. 2005. BSE agent signatures in a goat. *Vet. Rec.* **156**: 523–524. [Medline]
5. Fraser, H. and Dickinson, A. 1968. The sequential development of the brain lesions of scrapie in three strains of mice. *J. Comp. Pathol.* **78**: 301–311. [Medline] [CrossRef]
6. Hayashi, H. K., Yokoyama, T., Takata, M., Iwamaru, Y., Imamura, M., Ushiki, Y. K. and Shinagawa, M. 2005. The N-terminal cleavage site of PrP^{Sc} from BSE differs from that of PrP^{Sc} from scrapie. *Biochem. Biophys. Res. Commun.* **328**: 1024–1027. [Medline] [CrossRef]
7. Iwamaru, Y., Takenouchi, T., Ogihara, K., Hoshino, M., Takata, M., Imamura, M., Tagawa, Y., Hayashi-Kato, H., Ushiki-Kaku, Y., Shimizu, Y., Okada, H., Shinagawa, M., Kitani, H. and Yokoyama, T. 2007. Microglial cell line established from prion protein-overexpressing mice is susceptible to various murine prion strains. *J. Virol.* **81**: 1524–1527. [Medline] [CrossRef]
8. Kunkle, R. A., Nicholson, E. M., Lebepe-Mazur, S., Orcutt, D. L., Srinivas, M. L., Greenlee, J. J., Alt, D. P. and Hamir, A. N. 2008. Western blot detection of PrP^{Sc} in archived paraffin-embedded brainstem from scrapie-affected sheep. *J. Vet. Diagn. Invest.* **20**: 522–526. [Medline] [CrossRef]
9. Masujin, K., Matthews, D., Wells, G. A., Mohri, S. and Yokoyama, T. 2007. Prions in the peripheral nerves of bovine spongiform encephalopathy-affected cattle. *J. Gen. Virol.* **88**: 1850–1858. [Medline] [CrossRef]
10. Masujin, K., Shu, Y., Okada, H., Matsuura, Y., Iwamaru, Y., Imamura, M., Mohri, S. and Yokoyama, T. 2009. Isolation of two distinct prion strains from a scrapie-affected sheep. *Arch. Virol.* **154**: 1929–1932. [Medline] [CrossRef]
11. Nicholson, E. M. 2011. Enrichment of PrP^{Sc} in formalin-fixed, paraffin-embedded tissues prior to analysis by Western blot. *J. Vet. Diagn. Invest.* **23**: 790–792. [Medline] [CrossRef]
12. Nicholson, E. M., Kunkle, R. A., Hamir, A. N., Lebepe-Mazur, S. and Orcutt, D. 2007. Detection of the disease-associated isoform of the prion protein in formalin-fixed tissues by Western blot. *J. Vet. Diagn. Invest.* **19**: 548–552. [Medline] [CrossRef]
13. Peretz, D., Scott, M. R., Groth, D., Williamson, R. A., Burton, D. R., Cohen, F. E. and Prusiner, S. B. 2001. Strain-specified relative conformational stability of the scrapie prion protein. *Protein Sci.* **10**: 854–863. [Medline] [CrossRef]
14. Pirisinu, L., Migliore, S., Di Bari, M. A., Esposito, E., Baron, T., D'Agostino, C., De Grossi, L., Vaccari, G., Agrimi, U. and Nonno, R. 2011. Molecular discrimination of sheep bovine spongiform encephalopathy from scrapie. *Emerg. Infect. Dis.* **17**: 695–698. [Medline]
15. Prusiner, S. B. 1991. Molecular biology of prion diseases. *Science* **252**: 1515–1522. [Medline] [CrossRef]
16. Shimizu, Y., Kaku-Ushiki, Y., Iwamaru, Y., Muramoto, T., Kitamoto, T., Yokoyama, T., Mohri, S. and Tagawa, Y. 2010. A novel anti-prion protein monoclonal antibody and its single-chain fragment variable derivative with ability to inhibit abnormal prion protein accumulation in cultured cells. *Microbiol. Immunol.* **54**: 112–121. [Medline] [CrossRef]
17. Taylor, D. M., Brown, J. M., Fernie, K. and McConnell, I. 1997. The effect of formic acid on BSE and scrapie infectivity in fixed and unfixed brain-tissue. *Vet. Microbiol.* **58**: 167–174. [Medline] [CrossRef]
18. Telling, G. C., Parchi, P., DeArmond, S. J., Cortelli, P., Montagna, P., Gabizon, R., Mastrianni, J., Lugaresi, E., Gambetti, P. and Prusiner, S. B. 1996. Evidence for the conformation of the pathologic isoform of the prion protein enciphering and propagating prion diversity. *Science* **274**: 2079–2082. [Medline] [CrossRef]

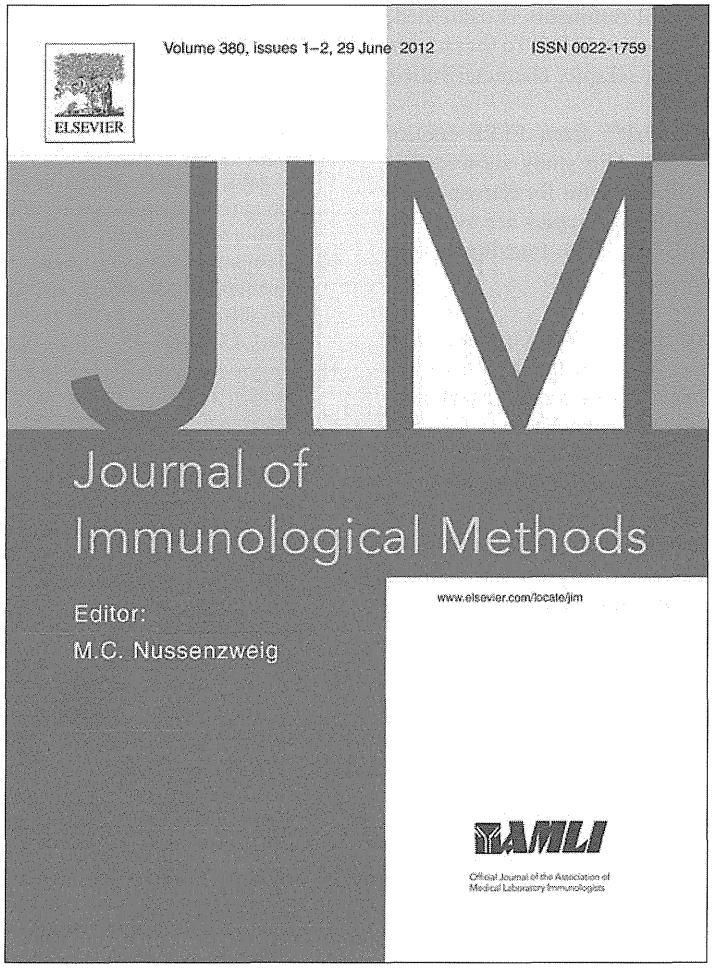

Journal of Immunological Methods 380 (2012) 30–39

Contents lists available at SciVerse ScienceDirect

Journal of Immunological Methods

journal homepage: www.elsevier.com/locate/jim

Research paper

All major prion types recognised by a multiplex immunofluorometric assay for disease screening and confirmation in sheep

Yue Tang [a,*], Adriana Gielbert [b], Jorg G. Jacobs [c], Thierry Baron [d], Olivier Andreoletti [e], Takashi Yokoyama [f], Jan P.M. Langeveld [c], Maurice J. Sauer [b]

[a] Department of Pathology & Host Susceptibility, Animal Health and Veterinary Laboratories Agency, Woodham Lane, New Haw, Addlestone, Surrey KT15 3NB, UK
[b] Department of Specialist Scientific Services, Animal Health and Veterinary Laboratories Agency, Woodham Lane, New Haw, Addlestone, Surrey KT15 3NB, UK
[c] Department of Infection Biology, Central Veterinary Institute of Wageningen UR, PO Box 65, 8200 AB Lelystad, The Netherlands
[d] Agence Francaise de Sécurité Sanitaire des Aliments – Lyon, Lyon, Cedex 07 69364, France
[e] UMR INRA ENVT 1225, Interactions Hôtes Agents Pathogènes, Ecole Nationale Vétérinaire de Toulouse, 31076 Toulouse, France
[f] National Institue of Animal Health,Tsukuba, Ibaraki 305-0856, Japan

ARTICLE INFO

Article history:
Received 28 October 2011
Received in revised form 14 March 2012
Accepted 21 March 2012
Available online 29 March 2012

Keywords:
Multiplex
Immunoassay
Differential diagnosis
Prion disease
Mass spectrometry

ABSTRACT

Prion diseases or transmissible spongiform encephalopathies (TSEs) in small ruminants are presented in many forms: classical scrapie, Nor98/atypical scrapie, CH1641 scrapie and bovine spongiform encephalopathy (BSE). We previously described a multiplex immunofluorometric assay (mIFMA), based on a bead array flow cytometry technology, which provided, in a single assay, discrimination between BSE (in cattle and sheep) and classical scrapie (Tang et al., 2010). In this study, we extended the mIFMA to differentiate classical scrapie, atypical scrapie, BSE (experimentally infected sheep and naturally infected cattle) and CH1641 (both experimental and natural CH1641-like infections in sheep). Three capture antibodies were used, two distinct PrP N-terminus specific antibodies 12B2 and 9A2, and a PrP core specific antibody 94B4. All three antibodies were shown to bind classical scrapie PrP^{res} strongly, whereas in Nor98/atypical scrapie PrP^{res} only 12B2 and 9A2 binding was observed. PrP^{res} binding of 12B2 was low for both BSE and CH1641, as expected.
Furthermore, analysis of serially diluted samples indicated that the assay provided a similar level of sensitivity for atypical scrapie as that found using a well established commercial test. Unexpectedly, 9A2 binding to CH1641 PrP^{res} was reduced by 2.1 fold both for experimental CH1641 and CH1641-like scrapie when compared with BSE, suggesting that major cleavage of the N-terminus occurs further towards the C-terminus in CH1641 than in BSE. The ratios of 12B2/94B4 and 9A2/94B4 were similar between experimental CH1641 and CH1641-like cases, although two CH1641-like subjects displayed slightly elevated ratios of both 12B2/94B4 and 9A2/94B4. To verify this finding for PrP^{res}, mass spectrometry based quantification was used to determine the absolute abundance of the peptides associated with all three antibody binding regions. There was a 2.2 fold reduction of peptides containing the 9A2 epitope for experimental CH1641 PrP^{res} in comparison to BSE PrP^{res}. Observation of reduced PrP^{res} may serve as a new marker for CH1641. This mIFMA may thus provide the basis for simplified TSE diagnosis with capability for simultaneous screening and differential diagnosis.

1. Introduction

Transmissible spongiform encephalopathies (TSEs), also called prion diseases, are neurodegenerative, infectious and fatal disorders (Prusiner, 1998). They include Creutzfeldt–

* Corresponding author.
E-mail address: yue.tang@ahvla.gsi.gov.uk (Y. Tang).

0022-1759/$ – see front matter.
doi:10.1016/j.jim.2012.03.004

Jakob disease (CJD) in humans, bovine spongiform encephalopathies (BSE) in cattle, scrapie in goats and sheep and chronic wasting disease in deer. Clinical disease and infectivity are associated with appearance of an abnormally folded isoform (PrP^{Sc}) of the normal host glycoprotein prion protein (PrP^{C}). This PrP^{Sc} is the diagnostic marker for prion infections. Prion diseases have long incubation periods prior to the onset of clinical signs. The hallmarks of TSEs in the central nervous system (CNS) include neuronal cell loss, vacuolation, gliosis and amyloid plaque formation, as well as deposition of PrP^{Sc} aggregates.

In the misfolded state, together with a concomitant aggregated nature of PrP^{Sc}, the prion protein partially resists proteinase K (PK) digestion, whereas PrP^{C} can be completely digested by protease treatment (Hill et al., 1998; Hope et al., 1999). The protease resistant product of PrP^{Sc} (PrP^{res}) has a ragged N-terminus (Gielbert et al., 2009), the N-terminal consensus sequence of which is TSE type dependent and allows differential diagnosis by biochemical methods (Hill et al., 1998; Stack et al., 2002; Thuring et al., 2004). For example, ovine N-terminal truncation of PrP^{res} from BSE is more extensive than that found for scrapie, judged by the lower average molecular mass of BSE PrP^{res} observed using western blotting analysis, indicative of the absence of the N-terminal PrP76-89 region (Thuring et al., 2004).

TSE types are often classified by the mouse bioassay (Ridley and Baker, 1997; Bruce, 2003). Histopathological and immunohistochemical (IHC) methods (Miller et al., 1993) are important confirmative tools (Spiropoulos et al., 2007) but as diagnostics they are unsuitable for large scale screening.

Current biochemical TSE isolate typing methods in sheep are largely reliant on assessment of the three characteristic Western blot bands representing the di-, mono-, and unglycosylated forms of PrP^{Sc} and PrP^{res}. The slightly lower mass of the unglycosylated band of BSE PrP^{res} enables experimental BSE in sheep to be distinguished from classical scrapie (Hill et al., 1998; Hope et al., 1999; Baron et al., 2000; Hunter and Houston, 2002; Stack et al., 2002; Nonno et al., 2003; Thuring et al., 2004). This small difference in truncation can be visualised more robustly and easily in brain and lymph nodes by WB epitope mapping of the N-terminus using prion protein antibodies with regional specificity for different sequence motifs (Thuring et al., 2004; Langeveld et al., 2006) and immunometric assay (Simon et al., 2008). More recently N-terminal amino acid profiling using Edman sequencing or mass spectrometry has presented the possibility of higher resolution differentiation by pinpointing the exact positions and extent of cleavage at these points (Hayashi et al., 2005; Howells et al., 2008; Gielbert et al., 2009). These practical procedures are most effectively applied to define and confirm strain type following a positive diagnosis from a high throughput non-discriminatory immunometric assay. Clearly the prospect of simultaneous routine testing and differential diagnosis by quantification of different crucial epitopes in the same sample aliquot would present substantial practical and cost advantages over two tiered, sequential approaches. In an ideal form, such a biochemical test would need to be capable of selectively detecting and quantifying several PrP epitopes within a given sample.

Flow cytometry principles have now been applied widely to the automated endpoint analysis of microwell immunofluorometric assays (IFMA) which allow detection of multiple different antibodies in a single tube (multiplex). In IFMA applications, multiple microbeads sets (arrays) are used, each with a distinct internal fluorescent signature and each attached to one of a range of capture antibodies with different epitope specificities; a mixture of these bead/antibody combinations can be readily distinguished by automated flow cytometry (Vignali, 2000; Dunbar, 2006). Thus, following multiplex IFMA using the bead/antibody array mixture, dual laser measurements of capture antibody bead and reporter antibody labels (e.g. phycoerythrin labelled second antibody or biotin tagged second antibody used with streptavidin-phycoerythrin) enables discrete identification and quantification of analyte (e.g. PrP^{res} types) binding to each capture antibody type (Fig. 1). Previous applications are numerous and include simultaneous testing of the immune response to foot-and-mouth disease associated non-structural proteins (Clavijo et al., 2006), detection and quantification of multiple cerebrospinal fluid biomarkers of Alzheimer's disease (Hansson et al., 2006) and multiplex detection of cytokines in antigen- and mitogen-stimulated human peripheral blood mononuclear cells (de Jager et al., 2003).

In the previous studies we developed a diplex immunofluorometric assay (IFMA) method to differentiate between classical scrapie and BSE (Tang et al., 2010). Here we describe the evolution of this approach, to provide a triplex assay (multiplex IFMA, or mIFMA) for differential diagnosis of all sheep TSE isolate types described to date: classical scrapie, atypical scrapie, BSE and even a rare scrapie variant typified by the isolate CH1641. These CH1641 isolates were derived both from experimental infections in sheep and one goat, and from ovine field cases with CH1641 like properties. It is particularly important to distinguish CH1641-like isolates because they share certain molecular characteristics with those of BSE, making differential diagnosis by biochemical methods particularly challenging (Stack et al., 2002; Baron et al., 2008).

2. Materials and methods

2.1. Chemicals and reagents

All chemicals were purchased from Sigma, Dorset, UK, unless otherwise specified, and were of at least analytical reagent grade. Streptavidin-R-phycoerythrin was purchased from Pierce (Rockford, IL, USA). Murine PrP monoclonal capture antibodies (mAbs) were produced at CVI (Langeveld et al., 2006): mAB 12B2 (IgG1) is selective for ovine PrP N-terminal amino acid residues ^{93}WGQGG^{97}, 9A2 (IgG1) for ^{102}WNK^{104} and 94B4 (IgG1) for ovine PrP C-terminal amino acid residues ^{190}HTVTTTTK^{197} (Fig. 1). The murine PrP mAb Sha31 (IgG1), (binding to ovine PrP core amino acid residues ^{148}YEDRYYRE^{155}), was purchased as ascites fluid (SPI-Bio, Montigny Le Bretonneux, France). Analogues of peptides representing relevant sequences of ovine PrP (Fig. S1) were custom synthesised (min. 98% purity; Peptide Protein Research Ltd., Eastleigh, UK) and used, for mass spectrometry method optimisation and as external calibration standards for mass spectrometry-based quantification.